國立交通大學
電子物理系所
碩士論文

碳、氮摻雜二氧化鈦粉末之室溫鐵磁性研究
Room temperature ferromagnetism in carbon, nitrogen doped TiO_2 powder

研究生：王家彬
指導教授：莊振益 教授

中華民國九十九年七月

碳、氮摻雜二氧化鈦粉末之室溫鐵磁性研究

Room temperature ferromagnetism in carbon, nitrogen doped TiO_2 powder

研究生：王家彬　　Student : Jia-Bin Wang
指導教授：莊振益 教授　　Adviser : Prof. Jenh-Yih Juang

國立交通大學
電子物理系所
碩士論文

A Thesis
Submitted to Department of Electrophysics
College of Science
National Chiao Tung University
in Partial Fulfillment of the Requirements
for Degree of Master
in
Electrophysics
July 2010
Hsinchu, Taiwan

中華民國九十九年七月

碳、氮摻雜二氧化鈦粉末之室溫鐵磁性研究

研究生：王家彬　　　　　指導教授：莊振益 教授

國立交通大學 電子物理學系碩士班

中文摘要

本研究中，我們利用固態燒結法製備摻雜碳、氮的二氧化鈦粉末，探討藉由非過渡金屬雜質所引發室溫鐵磁性的機制。我們發現摻雜碳、氮的二氧化鈦有很明顯的磁滯曲線，代表碳、氮可引發二氧化鈦在室溫時具有鐵磁性的現象。其鐵磁性的來源，推測是由氧空缺與雜質間相互作用所產生的。從 O-1s 的 XPS 可以看出，摻雜碳、氮可使氧空缺變多，而氧空缺產生的多餘電子。同時從 Ti-2p XPS 的變化發現一部分的電子與 Ti^{4+}產生電荷平衡變成 Ti^{3+}，另一部分的電子以自由電子的形式存在結構中以提供自旋極化的載子源。另外，二氧化鈦中同時存在碳(氮)雜質以及氧空缺，會發生類似 p-d 混成的 p-p 作用。進一步使能階分裂，在費米能階附近產生新

的空能態，當電荷轉移時就具有不成對的電子，成為自旋極化的來源。此一現象符合 Stoner criterion，亦即當費米能階附近的能態密度增加，因產生 Stoner splitting 而引發鐵磁性。總而言之，當二氧化鈦摻雜碳、氮使能階產生 Stoner splitting，提供起始的自旋極化，接著與氧空缺所產生的自由載子發生 exchange interaction，進而形成 Bound magnetic polarons (BMP)。當 BMP 有部分疊合透過自由載子產生進一步的 exchange interaction，使全部載子自旋方向排列成同方向而產生鐵磁性。

Room temperature ferromagnetism in carbon, nitrogen doped TiO_2 powder

Student : Jia-Bin Wang　　　Adviser : Prof. Jenh-Yih Juang

Department of Electrophysics
National Chiao Tung University

Abstract

In this study, we experimentally demonstrate that it is possible to induce room temperature ferromagnetism in carbon, nitrogen doped TiO_2 prepared simply by conventional solid state reaction method. From the magnetization hysteresis loop measurements, we can observe that N(C)-TiO_2 is ferromagnetic at room temperature. The origin of the RT-ferromagnetism is believed to intimately relate to the interaction of oxygen vacancies and impurities. From XPS spectra, nitrogen doping promotes the increasing loss of oxygen. Due to the charge balance requirement, the existence of oxygen vacancies partly transforms Ti^{4+} to Ti^{3+} and provides excessive electrons. When the impurities and oxygen vacancies are present simultaneously, it is anticipated to induce new states appearing near the Fermi level by p-p interaction. It not

only satisfies the Stoner criterion but also creates unpaired electrons. These unpaired electrons, in turn, act as the sources of spin-polarized carriers the eventually lead to room temperature ferromagnetism. Therefore, the p-p coupling interaction and charge transfer giving rise to the spin density near each impurity tends to align spin parallel to form moment at impurity ion. The moment-carrying impurities then strongly couples with carrier spins, generated by the existence of oxygen vacancies to form the bound magnetic polarons (BMP). If the concentration of BMPs is sufficiently high, it is able to effectively mediate the indirect ferromagnetic coupling among impurities by carries and result in ferromagnetism observed in the present system.

致謝

兩年，是長是短。兩年前的我與現今的我有何不同？還記得兩年前默默對自己期許，如今是否已經達到？雖然已被磨耗許多，但仍秉持當初的信念，往目標前行。不管最後是否能成功達成，已努力過，就不會留下遺憾。這兩年經過很多人的教導讓我成長許多，希望能往未來的路繼續邁前。

兩年的研究生活，要先感謝我的指導教授，莊振益教授。老師給予很高的自由度，讓我們可以做自己有興趣的實驗，探究箇中奧秘。還有林俊源、溫增明老師在實驗上給予的指導，以及吳光雄老師、朱英豪老師、羅志偉老師、陳錦明老師在研究上給予的建議，讓我受益良多。最後還要感謝在東華做專題時的指導教授，鄭嘉良教授。謝謝老師帶領我進入研究的殿堂，學習研究的方法，體會做研究的成就感，讓我在碩班能夠及早進入狀況，以創新的態度嘗試新的領域。

兩年的實驗室生活，要先感謝宗漢學長。在實驗上、儀器上都給予我很多建議與指導，讓我能夠順利完成實驗。還有昌學長、訓全學長、家宏學長、皓葦、培源、韋呈、凱婷、宗叡、長或在實驗方面的教導。當然還有同屆的夥伴俊宇、彥智、小賴、昱廷、嘉偉，不管在生活上還是研究上大家互相的幫忙。還有辦公室兩人組的前後團員，錦華和瀚云。你們大概是跟我待在辦公室最長時間的人，謝謝你們常跟我們聊天讓實驗室活絡許多。

最後還要感謝宗漢、昌學長、瀚云在未來工作上給了我很多意見，讓我對未來的工作不感徬徨。

兩年的交大生活，第一個要感謝的是我最好的朋友，姚欣佑。來到新竹你給我很多很多的幫忙，不管是生活上還是研究上你都赴湯蹈火。雖然每次跟你討論完實驗的東西，都讓我頭痛到不行，但還是非常感謝你願意花時間跟我討論，給我很多有用的建議，讓我的研究得以更加完備。這兩年我們也瘋狂做了很多蠢事，都讓人回味不已。還有從東華紅到交大來的東華四少，很懷念與你們吃飯聊天回味以前的大學生活，很感謝你們兩年來的陪伴。還有在清大的助理小姐，Dino。很感謝你在實驗上給予的幫忙與意見，還有每次的聚會都麻煩你聯絡難搞的大家，謝謝你啦~～

二十四個年頭，我已完成人生的第一個階段。最要感謝我的家人，是你們給了我動力，讓我努力不懈；是你們給了我勇氣，讓我奮發前行；是你們給了我關懷，讓我不感孤單；是你們給了我歡樂，讓我充滿活力；是你們給了我支持，讓我擁有自信；是你們給了我愛，讓我的人生得以完全。

謝謝你們~～

感恩合十~～

家彬

Contents

List of Figures

Chapter 1

Introduction

1-1 Magnetic materials v.s Semiconductor

The possibilities of integrating the existing semiconductor technologies with novel magnetic materials have intrigued scientists for a long time, owing to the seemingly unlimited application potential such combination has to offer. The spin property of electrons has been successfully utilized to achieve useful magnetic device, such as magneto-optical recording device, magneto-resistance read head and magnetic sensor. On the other hand, numerous electronic devices used in semiconductor industry, i.e. integrated circuits (ICs), transistors or lasers and light emitting diodes, transmit complex information by controlling the behavior of the carriers in semiconductors. The breakthrough of magnetic and semiconductor science gives rise to the rapid developments of computer technique and communication integrity. However, the traditional semiconductor electronic devices suffer from several problems: slow speed of signal transmission, low efficiency resulting from energy dissipation and too large size of device for applications. Those drawbacks are primarily originated from the limitation of mobility and serious collisions of carriers in semiconductors. Moreover, in order to explore higher performance, the size of semiconductor devices has to be decreased to submicron or nano size. The effects of exchange interaction between carriers can become a more important factor in the devices. So if the signal transmission process is accomplished by controlling of the orientation and the coupling between different spin states, the corresponding signal speed will become relatively faster with smaller energy dissipation. Therefore, how to take the advantages of well-developed technologies in traditional semiconductors and incorporate spin mechanism to design advanced devices has become an important issue. Those kinds of devices are called spin transport electronic (spintronic) system, such as magneto-resistance random access memory, spin-FET and spin-LED, optical isolator and quantum computer. Consequently, study the fundamental physics of magnetism and search for new magnetic materials to develop the useful spintronic devices will certainly be the main-stream trend in the future [1,2].

As the researches of spintronics evolve, three important tasks arise: efficient spin injection, overall spin control and spin detection, which play the important roles in the improvement of spintronic-device performance. In early stages, many researches focused on searching the high spin-polarized material for the purpose of high-efficiency spin injection. Due to the nature ferromagnetism of most transition metals, many studies have been devoted to combine the transition metals and traditional semiconductors by delicate growth technologies. However, the mismatching between the crystal geometries of these two kinds of materials has limited the efficiency of spin-injection process. In other words, this approaching has been not very successful, because of the great geometrical and chemical-property differences between the transition metals and traditional semiconductors. On the other hand, in 1960, “*concentrated*” magnetic semiconductors, such as europium chalcogenides (rock-salt type ex: EuSe and EuO) were proposed. These kinds of materials were also called ferromagnetic semiconductors, which possess the fundamental characteristics of ferromagnetism and traditional semiconductor. A ferromagnetic semiconductor contains numerous spin-polarized carriers; hence the motion and the spin states of the carriers can be easily controlled by the electromagnetic field (EM field). Manipulation of the interaction between the charges (carriers) and photons provides the controllability of not only the magnetism, but also the behavior of semiconductor. Nevertheless, the Curies temperature (T_c) of ferromagnetic semiconductor is usually lower than 100K. Moreover, this kind of material is also very difficult to form the hetero-structures. These two drawbacks have resulted in the severe limitations of its practical applications. Furthermore, two types of new promising magnetic materials with high spin-injection efficiency have appeared in recent decades. The first one is called "*half-metal*", which possesses 100% spin polarization, such as CrO_2, mixed valence maganties (($La_{1-x}A_x$)MnO_3 (x～0.3, A=S r, Ca, Ba)), Fe_3O_4, and double perovkites (A2BB\`O6 (A = Sr, Ca, Ba，B = Fe, Co，B\`= Mo, Re)) [3~8]. Although these magnetic materials indeed possess the characteristic of 100% spin polarization, but it is difficult to produce heterogeneous structures, so have restricted the application. Another one is the so-called "diluted magnetic semiconductors" (DMSs) realized by doping transition metals into traditional semiconductors. The doped transition metal induces the unpaired electrons which lead to the intrinsic spontaneous spins in the semiconductor system. The detail of DMSs will be further discussed in later sections. In summary, functional ferromagnetic semiconductors plays the key role in the development of spintronic devices, therefore, studying the underlying physics and fundamental mechanism of these ferromagnetic semiconductors becomes an important issue.

1-2 What are diluted magnetic semiconductors?

The traditional diluted magnetic semiconductors (DMSs) are semiconductors in which a fraction of the host cations can be substitutionally replaced by magnetic ions or appropriate rare earths. Such a compound (Fig. 1-1-1(b)) can be regarded as an alloy between a non-magnetic semiconductor (Fig. 1-1-1(c)) and a magnetic semiconductor (Fig. 1-1-1(a)). Transition metals (TMs) that have partially filled *d* states (Sc, Ti, V, Cr, Mn, Fe, Co, Ni, and Cu) and rare earth elements (e.g. Eu, Gd, Er), which have partially filled f states, have been used as magnetic atoms in DMS. The partially filled *d* states or *f* states contain unpaired electrons, which are responsible for their magnetic behaviors.

Since the crystal structure and chemical bond of DMSs match well with available semiconductor devices and the band exhibits Zeeman splitting at temperatures lower than Tc, so that it can induce huge spin polarization serves as the source of spin polarization in spintronic devices. Even more importantly, to obtain such electronic devices operational at room temperature is the necessary condition for all practical purposes. Indeed, a ferromagnetic response persisting up to above room temperature has been the highlighted issues and opportunities arising in this corner of solid state science.

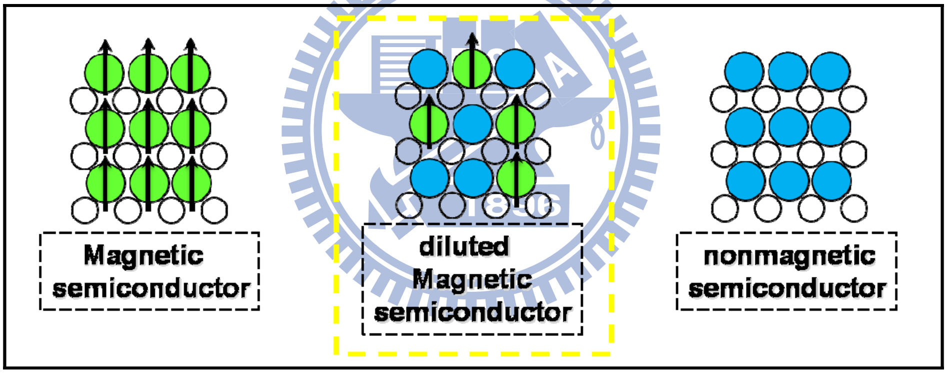

Fig. 1 The different types of semiconductors: (A) a magnetic semiconductor; (B) a DMS and (C) a non-magnetic semiconductor.

1-3 The review of magnetic semiconductors

The theoretical prediction and observation of room temperature ferromagnetism in doped transition metal DMSs is one of the most interesting scientific developments of the early 21st century. DMSs typically consist of a nonmagnetic semiconductor doped with transition metal elements which possess unpaired d or f electrons. These unpaired electrons can form the local magnetic moments and the coupling between them may result in collective magnetism.

1-3.1 Traditional DMS

In 1980s, DMSs, i.e. semiconductor doped with diluted magnetic atoms, gradually attracted considerable attention. Most of studies have been focused on the II-VI compounds, such as (Cd or Mn)Te、(Zn or Mn)Te、(Zn or Co)S、(Hg or Fe)Se. Though high density of magnetic atoms can be doped into the II-VI compounds, n- or p- type doping carrier concentration remains relatively low due to the similar valences of transition metal elements and the cation of II-VI compounds. Thus, despite of the matured doping technique of II-VI DMS compounds accomplished by using molecular beam epitaxy (MBE), the p-type doping II-VI (Cd, Mn)Te, (Zn, Mn)Te and (Be, Mn)Te only exhibited ferromagnetism with Tc below 10K. These kinds of II-VI ferromagnetic semiconductors are therefore unsuitable for spintronic devices for operating at RT.

For III-V DMSs, like $Mn_xGa_{1-x}As$, Mn contributes both the magnetic moment and the hole carriers (i.e. p-type DMS). Both turn out to be equally important for obtaining ferromagnetism within the framework of the mean-field approximation (MFA) [9], there are two basic assumptions in the theory:

1. The ferromagnetism originates from the indirect interaction of localized magnetic moments of doping magnetic atoms, that is to say, the ferromagnetism is induced by the hole carriers (carrier-induced ferromagnetism).
2. The long distance spin-spin interaction.

For this case, the Mn ions are acceptors and generate holes in the valence bands. These holes antiferromagnetically interact with the Mn ions and lead to the indirect coupling between the neighboring Mn and Mn ions to become ferromagnetic. According to the mean-field theory, the Tc increases with the concentration of Mn doping and hole concentration. It is noted that the hole carriers are created by the Mn atoms replacing some of the Ga atoms in GaAs. However, the concentration of hole is far below the concentration of doping Mn atoms observed in many experiments. As a sequence, the Mn atoms may have acted as compensating donors and decrease the hole concentration, leading to a decrease of Tc.

A theoretical prediction by Dietl et al. [10] demonstrates that the Curie temperature can be increased above room temperature in p-type semiconductor based DMSs (Fig.2). The calculations also show that ferromagnetism is stable in a DMS which is based on a wide bandgap semiconductor. Moreover, the recent reports of room temperature in p-type ferromagnetism in ZnO-based semiconductors [11] as well as in Co:TiO_2 oxide films [12] have encouraged intensive experimental studies to look into oxide-based DMSs (O-DMSs).

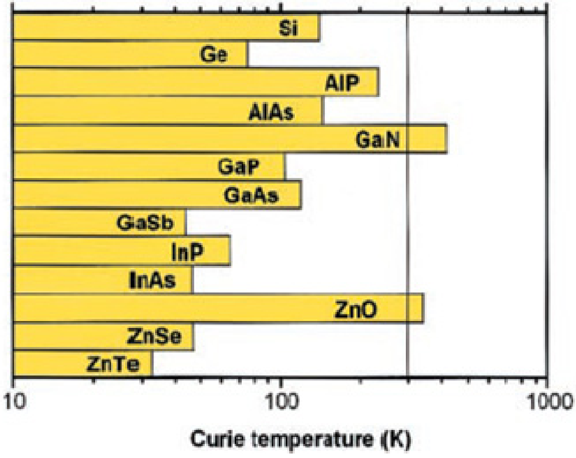

Fig. 2 The Curie temperature of numerous p type DMS predicted by mean-field approximation theory.(Mn doping concentration : 5% and hole concentration : $3.5\times10^{20}/cm^3$). The black line indicates room temperature (300K) [10].

Even though ferromagnetism has been observed in a number of systems, experimental studies on TM-doped O-DMSs have resulted in inconsistent results and the mechanism giving rise to the room-temperature ferromagnetism in TM-doped O-DMSs remains unclear. For instance, Chamber et al. [13] found the Co clusters existing in Co doped TiO_2 film and argued that the observed ferromagnetism may have come from the contribution of the Co clusters. Punnoose et al. [14] and Kennedy et al. [15] also found the presence of Co clusters in different experiments. The inability of excluding the ferromagnetism seen in TM-doped O-DMSs form cluster or secondary phases has hindered the application of DMSs. The revived search for DMSs was based on alternative dopants. If non-TM dopants can be incorporated in O-DMSs and induces magnetism, it should be able to clarify the source of ferromagnetism. These have been called d^0 magnetism, indicating that no ions with partially filled d-shell are at the origin of the magnetic moments. For example, copper doping in ZnO and GaN have been investigated and it has been confirmed experimentally both Cu-doped ZnO and GaN are room-temperature ferromagnetic DMSs [16~19].

Recently several groups have found room temperature ferromagnetism in N-doped ZnO and C-doped ZnO film [20~23]. The existing traditional theories of DMS cannot be applied to the d^0 magnetism, because they are based on the existence of the d and f orbitals, but there are no such orbitals in these 2p-light element doped materials. Moreover the mechanism for ferromagnetism in such anion doped magnetic materials is still not clear.

Among the oxide based DMS materials, TiO_2 and ZnO are the most interesting semiconductor materials due to their potential for industrial application and thus have received much attention. Thus, we will present a brief review on TiO_2 and the 2p-light element doped DMSs.

1-3.2 TiO_2-based materials:

Since 2001, many publications dealing with the growth and properties of magnetically doped transition metal oxides have appeared. Matsumoto et al. [24,25]

used a combinatorial approach with pulsed laser deposition (PLD) to grow TiO_2 films in both anatase and rutile forms and doped them with the first row transition metal from Sc to Zn. Each was screened for ferromagnetism using a superconducting quantum interface device (SQUID) magnetometer. Among these many combinations, only epitaxial Co-doped TiO_2 anatase grow on $LaAlO_3$ (001) was found to exhibit room temperature ferromagnetism (Tc>400K). On the other hand, other growth methods such as oxygen plasma assisted molecular beam epitaxy (OPAMBE) [26~30], sputtering [31,32] and direct chemical nanocrystal and nanorod synthesis [33,34], have been used to synthesize true Co-doped TiO_2 anatase. The as-grown OPAMBE growth material was found to be FM at room temperature with a moment of ~1.1 μ_B per Co. The nanocrystals and nanorods growth by direct chemical methods were paramagnetic in as-grown conditions, but became strongly ferromagnetic (～up to 1.9 μ_B per Co) when spin coated onto a polycrystalline sapphire substrate and annealed in air at 350℃. But a number of studies [35, 36] indicate that the RT ferromagnetism in TM-doped oxides may come from magnetic clusters or secondary magnetic phases, for example as shown in Fig. 3. On the other hand, there are reports suggest the absence of magnetic clusters or secondary phases and support intrinsic ferromagnetic origin. So far, the origin of ferromagnetism remains a very controversial topic.

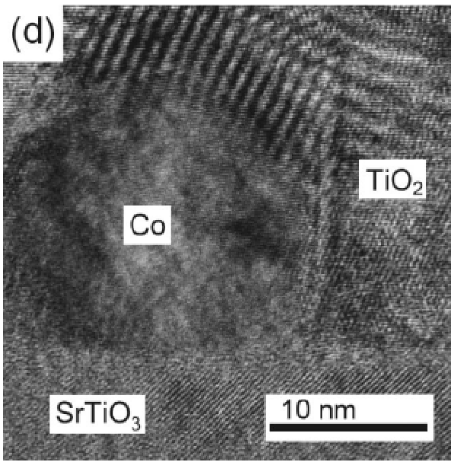

Fig. 3 A high resolution XTEM picture of the nanoclustered film near the film/substrate interface. [35]

Punnoose et al. [14] reported detailed studies of temperature dependent magnetization (M(T)) at H=50 Oe with zero-field-cooled (ZFC) and field-cooled (FC) schemes and showed that M(T) peaks at T_p~30K for 1% Co and T_p~125K for 12% Co doped films, respectively. Nevertheless, it was pointed out that bifurcation of FC and ZFC M(T) curves, shown in Fig.4 are typical feature of a blocked nanoparticle system. Thus it is due most likely to the contributions from the Co nanoparticles in the Co/TiO_2 samples. Therefore, the existence of cluster or second phase has been a problem in TM-doped DMS.

Recently, several groups have found room temperature ferromagnetism (RTFM) in undoped HfO_2, In_2O_3, ZnO, and SnO_2 films [37~41]. It is believed that the FM in undoped TiO_2 films originates from the oxygen vacancies (V_o) localized near the film-substrate interface by analyzing FM in samples prepared under different conditions [38~45] and FM in samples with different thicknesses [41~43,45].

For example, data of the oxygen annealed films of TiO_2 and HfO_2 [38] are shown in Fig.5 along with the data of as-deposited films in order to be compared directly. This evidence has clearly indicated the primary role played by oxygen vacancies. Nevertheless, the mechanisms to explain how FM emerges are contradictory. It is amazing that undoped oxides DMS possess ferromagnetism at room temperature because it challenges the “traditional” picture in explaining TM-doped DMSs. First of all, according to the general theory of magnetism, if there is no unpaired d or f electrons, there will be no ferromagnetism. Thus, although the term “d^0 magnetism” has been brought about to explain the phenomena, the mechanism of d^0 magnetism is still not clear, and should be an interesting issue in the future.

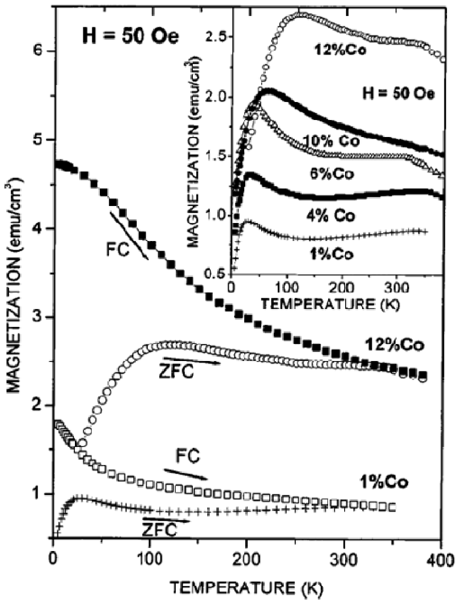

Fig. 4 Temperature variations of the magnetization for ZFC and FC cases for the 1% and 12% Co samples. The inset shows ZFC data for the five Co concentrations.

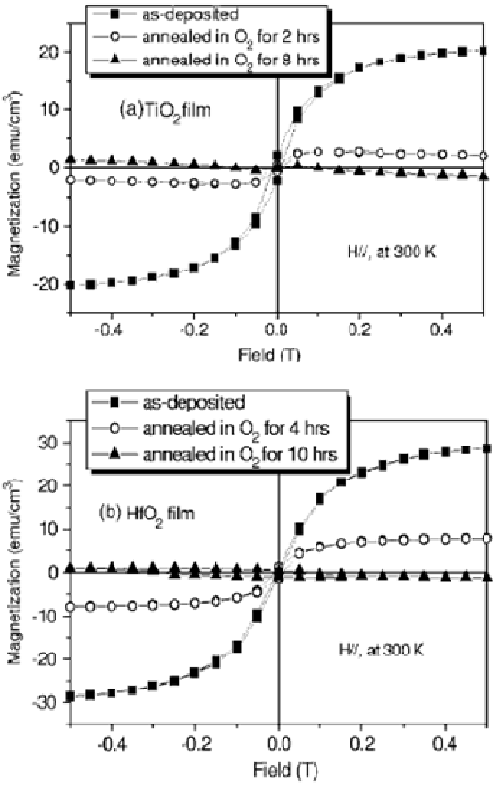

Fig. 5 M-H loops taken at 300 K for (a) TiO_2 films as-deposited, annealed in O_2 at 650 °C for 2 h and for 8 h and (b) HfO2 films as-deposited, annealed in O_2 at 800 °C for 4 h and for 10 h.

1-3.3 2p-light element doped DMSs :

Several groups have found room temperature ferromagnetism in N-doped ZnO and C-doped ZnO film [49~52], in which nitrogen and carbon are substitutes for oxygen. The existing theories of traditional DMS cannot be applied to 2p light element-doped DMS, but the 2p light elements appear to be ideal impurities to produce ferromagnetism in these materials. It is believed that the valence electrons in p states are more delocalized hence have much larger spatial extensions which, in turn, could promote long-range exchange coupling interactions. Therefore, DMSs doped with 2p light elements can be weak ferromagnets in a highly ordered and low doping concentration [53]. Pan, et al. believed that substitution of N or C atoms at the O sites in ZnO introduces holes in O 2p states, which couple with the parent N 2p or C 2p localized spins by the p-p interaction, leading to effects similar to p-d hybridization in TM-doped DMSs. Based on first-principle density functional theory (DFT) calculations, the C-doped anatase TiO_2 may induce ferromagnetism when some O atoms are substituted by C atoms [54]. In that, each C has spin-polarized 2p states in the band gap generating a magnetic moment of $2.0\mu_B$.

Moreover, based on the first-principle calculations, Rumaiz et al. [55] deemed that N doping of TiO_2 leads to the formation of oxygen vacancies and results in an impurity state at the Fermi energy. Besides, Coey et al. [56] proposed a model for the ferromagnetism of doped oxide nanoparticales and related materials. Basically, the defective oxides are presumed to be the Stoner ferromagnets; the spontaneous Stoner ferromagnetism can arise in percolating defect-rich regions where charge transfer happens. Therefore, the 2p-light elements can be better alternatives for impurities to produce ferromagnets in oxide semiconducting materials.

1-4 Motivation

From the above survey, we note that both C-and N-doping to TiO_2 may lead to Stoner ferromagnets and can be excellent candidates for DMS for RTFM. We also note that most of the researches on 2p-light element doped DMSs have been focused on films, which inevitably incorporates unexpected defects from processes that may complicate the interpretations of the obtained results. Thus, it may be significant and instructive to investigate FM in 2p-light element DMSs powders because they might reflect intrinsic magnetic properties of materials. Therefore, in this study, we try to prepare TiO_2 powder with nitrogen and carbon dopants in order to clarify some of the issues stated above.

Chapter 2

Background

2-1 Spin interaction in DMS

In this section, we describe the models that are most commonly used to describe the magnetic interactions in diluted magnetic semiconductors.

(I) Origin of exchange [57]

Consider a simple model with just two electrons which have spatial coordinate $\mathbf{r}_1$ and $\mathbf{r}_2$ respectively. The wave function for the joint state can be written as a product of single electron states, so that if the first electron is in state $\psi_a(\mathbf{r}_1)$ and the second electron is in state $\psi_b(\mathbf{r}_2)$, then the joint wave function can be written as $\psi_a(\mathbf{r}_1)\psi_b(\mathbf{r}_2)$.

For electrons the overall wave function must be antisymmetric so the spin part of the wave function must either be an antisymmetric singlet state χ_S (S = 0) in the case of a symmetric spatial state or a symmetric triplet state χ_T (S = 1) in the case of an antisymmetric spatial state. Therefore we can write the wave function for the singlet case Ψ_S and the triplet case Ψ_T as

$$\Psi_s = \frac{1}{\sqrt{2}}[\psi_a(\mathbf{r_1})\psi_b(\mathbf{r_2}) + \psi_a(\mathbf{r_2})\psi_b(\mathbf{r_1})]\chi_S$$

$$\Psi_T = \frac{1}{\sqrt{2}}[\psi_a(\mathbf{r_1})\psi_b(\mathbf{r_2}) - \psi_a(\mathbf{r_2})\psi_b(\mathbf{r_1})]\chi_T$$

where both the spatial and spin parts of the wave function are included. The energies of the two possible states are

$$E_S = \int \psi_S^* \hat{H} \psi_S^* d\mathbf{r}_1 d\mathbf{r}_2$$

$$E_T = \int \psi_T^* \hat{H} \psi_T^* d\mathbf{r}_1 d\mathbf{r}_2$$

with the assumption that the spin parts of the wave function χ_S and χ_T are normalized. The difference between the two energies is

$$E_S - E_T = 2\int \psi_a^*(\mathbf{r_1})\psi_b^*(\mathbf{r_2})\hat{H}\,\psi_a(\mathbf{r_2})\psi_b(\mathbf{r_1})dr_1dr_2$$

For a singlet state $\mathbf{S}_1 \cdot \mathbf{S}_2 = -3/4$ while for a triplet state $\mathbf{S_1} \cdot \mathbf{S_2} = 1/4$. Hence the Hamiltonian can be written in the form of an "effective Hamiltonian"

$$\hat{H} = \frac{1}{4}(E_S + 3E_T) - (E_S - E_T)S_1 \cdot S_2$$

This is the sum of a constant term and a term which depends on spin. The constant can be absorbed into other constant energy terms, but the second term is more interesting. The exchange constant (or exchange integral), J is defined by

$$J = \frac{E_S - E_T}{2} = \int \psi_a^*(\mathbf{r_1})\psi_b^*(\mathbf{r_2})\hat{H}\,\psi_a(\mathbf{r_2})\psi_b(\mathbf{r_1})dr_1dr_2$$

and hence the spin-dependent term in the effective Hamiltonian can be written

$$\hat{H}^{spin} = -2JS_1 \cdot S_2$$

If $J > 0$, $E_S > E_T$, the triplet state $S = 1$ is favored. On the other hand, if $J < 0$, $E_S < E_T$, the singlet state $S = 0$ is favored. This equation is relatively simple to derive for two electrons, but generalizing to a many-body system is far from trivial. This motivates the Hamiltonian of the Heisenberg model:

$$\hat{H} = -\sum_{ij} J_{ij}\, S_1 \cdot S_2$$

where J_{ij} is the exchange constant between the i^{th} and j^{th} spins.

(II) Direct exchange

If the electrons on neighboring magnetic atoms interact via an exchange interaction, this is known as direct exchange. This is because the exchange interaction proceeds directly without the need for an intermediary. Though this seems to be the most obvious route for the exchange interaction to take, the reality in physical situations is rarely that simple. Very often direct exchange cannot be an important mechanism in controlling the magnetic properties because there is insufficient direct overlap between the orbitals of the neighboring magnetic ions.

(III) Superexchange

Superexchange can be defined as an indirect exchange interaction between non-neighboring magnetic ions which is mediated by a non-magnetic ion which is placed in between the magnetic ions. It arises because there is a kinetic energy advantage for antiferromagnetism, which can be understood by referring to Fig. 6(a) which shows two transition metal ions separated by an oxygen ion. For simplicity we will assume that the magnetic moment on the transition metal ion is due to a single unpaired electron (more complicated cases can be dealt with in analogous ways). Hence if this system were perfectly ionic, each metal ion would have a single unpaired electron in each d orbit and the oxygen would have two p electrons in its outermost occupied states. The figure demonstrates that antifcrromagnetic coupling lowers the energy of the system by allowing these electrons to become delocalized over the whole structure, thus lowering the kinetic energy.

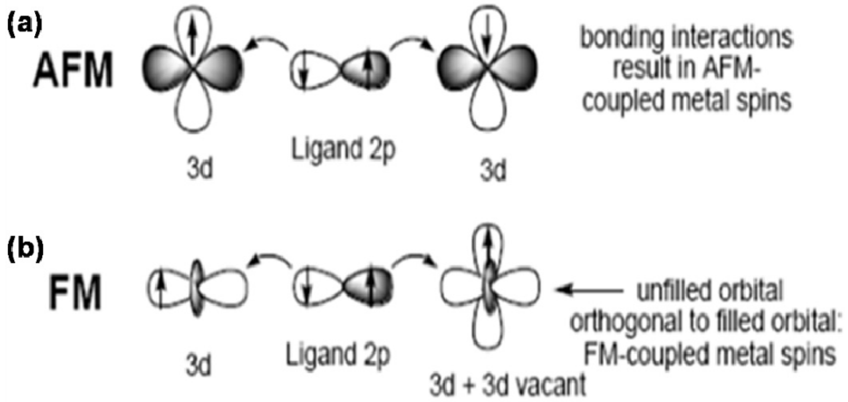

Fig. 6 Depict the hoping processes of the superexchange.

(IV) Double exchange

In some oxides, it is possible to have a ferromagnetic exchange interaction which occurs because the magnetic ion can show mixed valence, which is it can exist in more than one oxidation state (Fig. 6(b)). Examples of this include compounds containing the Mn ion which can exist in oxidation state 3 or 4, i.e. as Mn^{3+} or Mn^{4+} (Fig. 7). The e_g electron on a Mn^{3+} ion can hop to a neighboring site only if there is a vacancy there of the same spin (since hopping proceeds without spin-flip of the hopping electron). If the neighbor is a Mn^{4+} which has no electrons in its e_g shell, this should present

no problem. However, there is a strong single-centre exchange interaction between the e_g electron and the three electrons in the t_{2g} level which wants to keep them all aligned. Thus it is not energetically favourable for an e_g electron to hop to a neighboring ion in which the t_{2g} spins will be antiparallel to the e_g electron (Fig. 7(b)). Ferromagnetic alignment of neighboring ions is therefore required to maintain the high-spin arrangement on both the donating and receiving ion. Because the ability to hop gives a kinetic energy saving, allowing the hopping process shown in Fig. 7(a) reduces the overall energy. Thus the system favors to align ferromagnetically and saves energy.

The physics of this mechanism is applied to mixed-valence DMSs, i.e. semiconductors in which one can find coexisting magnetic ions of the same chemical nature but with different charge states. The magnetic ions with different charge states were also observed in III–V DMS [58]. Although it is believed that in GaAs and InAs the Mn ions are in the high spin 2^+ charge state [59, 60], the precise nature of the charge state related to Mn ions is not finally determined in these materials. Recently, the coexistence of Mn^{2+} and Mn^{3+} ions leading to double exchange induced ferromagnetism was also suggested in ZnO [61].

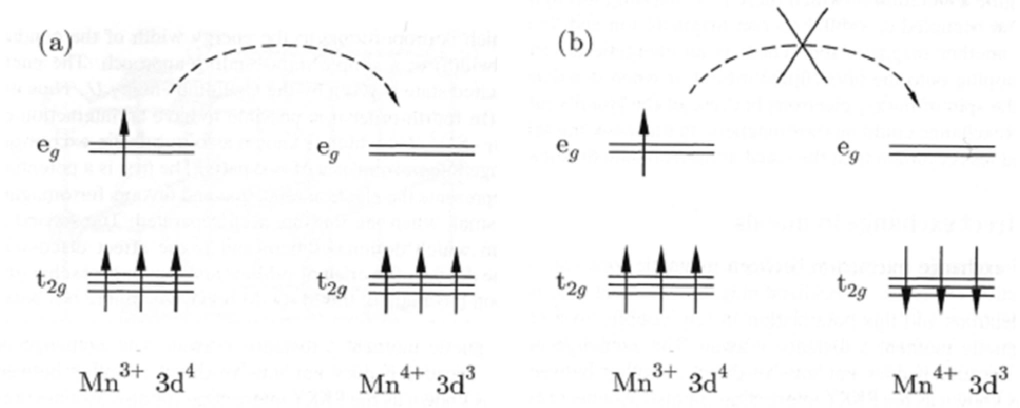

Fig. 7 Schematics that depict the hoping processes of the double exchange.

2-2 Spontaneous spin-split band [57]

It is evidently demonstrated that band ferromagnetism in which the magnetization is due to spontaneously spin-split bands might also play a role for ferromagnetism exhibited in some DMSs. In this section we will explore some models which might be relevant to understand how energy bands in some materials can become spontaneously spin-split.

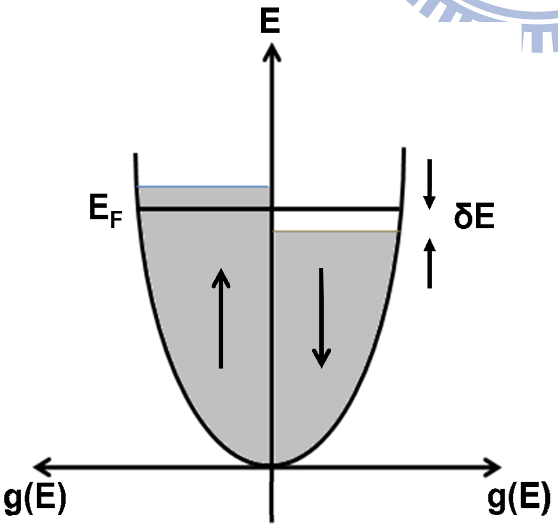

Fig. 8 Density of states showing spontaneous splitting of energy hands without an applied magnetic field.

In the absence of an applied magnetic field, if we take a small number of electrons near the Fermi surface from the spin-down band and place them in the spin-up band, one immediately sees the imbalance between the spin-up and spin-down bands will lead to magnetism. Specifically, if we take spin-down electrons with energies from $E_F — \delta E$ up to E_F and flip their spins, placing them in the spin-up band where they sit with energies from E_F up to $E_F + \delta E$, as schematically illustrated in Fig. 8. The number of electrons moved is $g(E_F)\delta E/2$ and they increase in energy by δE. The total energy change is $g(Ep)\delta E /2 \times \delta E$. The total kinetic energy change $\Delta E_{K.E.}$ is therefore

$$\Delta E_{K.E.} = \frac{1}{2} g(E_F)(\delta E)^2$$

This is an energy cost so this process looks unfavorable. However, the interaction of the magnetization with the molecular field gives an energy reduction which can outweigh this cost. The number density of up-spins is $n^{\uparrow} = \frac{1}{2}(n + g(E_F)\delta E)$ and the number density of down-spins is $n^{\downarrow} = \frac{1}{2}(n - g(E_F)\delta E)$. Hence the magnetization is $M = \mu_B(n^{\uparrow} - n^{\downarrow})$, assuming each electron has a magnetic moment of $1\mu_B$. The molecular field energy is

$$\Delta E_{M.F.} = -\int_0^M \mu_0(\lambda M')\, dM' = -\frac{1}{2}\mu_0\lambda M^2 = -\frac{1}{2}\mu_0\mu_B^2\lambda(n^{\uparrow} - n^{\downarrow})^2$$

Writing $U = \mu_0\mu_B^2\lambda$ where U is a measure of the Coulomb energy, we have

$$\Delta E_{M.F.} = -\frac{1}{2} U (g(E_F)\delta E)^2$$

Hence the total change of energy ΔE is

$$\Delta E = \Delta E_{K.E.} + \Delta E_{M.F.} = \frac{1}{2} g(E_F)(\delta E)^2 \big(1 - U g(E_F)\big)$$

Thus spontaneous ferromagnetism is possible if $\Delta E < 0$, which further implies that

$$U g(E_F) \geq 1$$

This condition is known as the **Stoner criterion**. This condition for the ferromagnetic instability requires that the Coulomb effects are strong and also that the density of states at the Fermi energy is large. If there is spontaneous ferromagnetism, the spin-up and spin-down bands will be split by an energy A, where A is the exchange splitting, in the absence of an applied magnetic field.

2-3 Bound magnetic polarons

In the BMP model, oxygen vacancies act both as electron donors and as electron traps which can bind the electrons and maintain insulating behavior. Each trapped electron couples to the local moments of the host lattice that lie within its orbit ferromagnetically, leading to a bound polaron with a large net magnetic moment.

If neighboring BMPs do not interact strongly with each other, a paramagnetic, insulating phase results. However, for certain BMP–BMP distances and combinations of electron–electron and electron–local moment exchange constants, the BMPs may couple in a ferromagnetic fashion [62, 63]. The critical distance at which the exchange between two BMPs becomes ferromagnetic is typically of the order of a few Bohr radii [63]. The amplitude of the exchange interaction then drops off rapidly with distance. Above some critical electron density, the attractive potential of the vacancy is screened, the donor electrons become unbound, and the system becomes metallic [64] and, depending on the temperature, can be either paramagnetic or ferromagnetic.

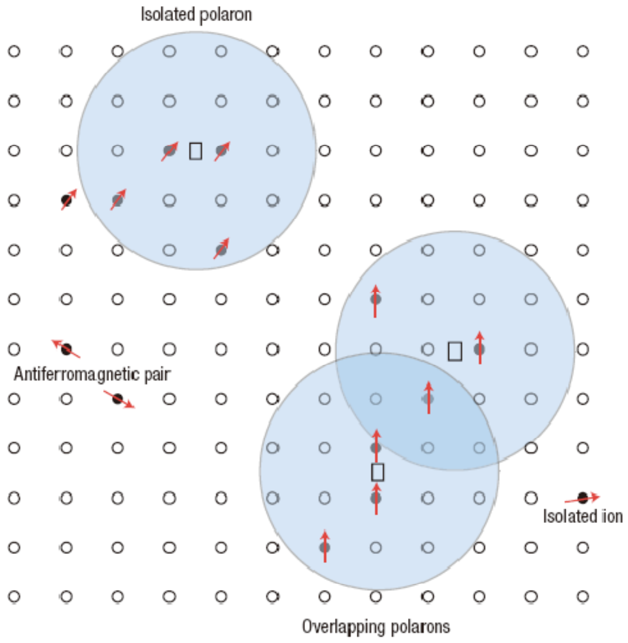

Fig. 9 Representation of magnetic polarons. Cation sites are represented by small circles. Oxygen is not shown; the unoccupied oxygen sites are represented by squares [65].

The spin-split donor impurity-band model originated from oxygen vacancies constituted magnetic BMP has been used to explain the observed variation of magnetic moments across the TM-doped ZnO series, as shown in Fig. 10. On passing along the 3d series from Ti to Cu, the spin-split d levels move down in energy towards the top of the oxygen 2p-band. Hence there are two regions where a high *Tc* is expected: one near the beginning of the series where the $3d_\uparrow$ states cross the Fermi level in the impurity band, and one towards the end where the $3d_\downarrow$ states cross the Fermi level. For the light 3d elements, the $3d_\uparrow$ states lie high in the 2p (O) and 4s (Zn) gap, overlapping the donor impurity band which is spin split. In the middle of the series, there is no overlap with the 3d levels and exchange is weak, but towards the end of the series the $3d_\downarrow$ states overlap the impurity band, which then has the opposite spin splitting for the same occupancy. High *Tc* is found whenever unoccupied 3d states overlap the impurity band, but not otherwise.

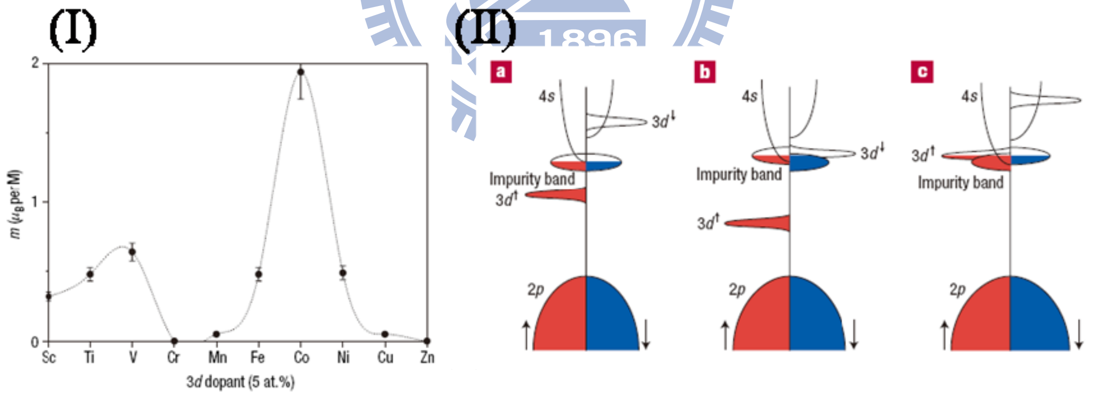

Fig.10 (I) The magnetic moment of thin films produced from ($Zn_{0.95}M_{0.05}$)O targets by pulsed-laser deposition, for M = Sc – Cu, measured at room temperature.
(II) Schematic band structure of an oxide with 3d impurities and a spin split donor impurity band. (a) The position of the 3d level for low Curie temperature, when the splitting of the impurity band is small. b, and c, show positions of the minority (b) or majority-spin (c) 3d bands, respectively, which lead to high T_C[65].

Chapter 3

Experiments

3-1 Sample preparation

We experimentally demonstrate that it is possible to induce room temperature ferromagnetism in 2p-light-element doped TiO_2 prepared simply by conventional solid state reaction method. We divide our experiment into two part, one is to anneal the high purity rutile TiO_2 (99.998%) powders twice under different nitrogen pressures at 1273K for 2hours. The other is utilized high purity TiO_2 to mix with carbon (99.999%) powders. The mixtures were then heated at 1273K for 6 hours under a reduced pressure of $<6x10^{-4}$ torr to promote reactions among the mixing constituents. The solidified mixture was then grinded and pressed using a mold to form the target body; the target body was heated twice at 1273K for 12 hours. This step is intended to increase the contact area between carbon and TiO_2 powders. Care was taken to prepare sample from directly contacting any ferrous tools or vessels during synthesis and characterization processes. Structural and magnetic characterizations of 2p-doped TiO_2 samples were carried out by means of x-ray diffraction (XRD), x-ray photoelectron spectroscopy (XPS), superconducting quantum interference device (SQUID), and electron paramagnetic resonance (EPR).

3-2 Measurements

(I) X-ray diffraction (XRD)

X-ray diffraction is a common technique for studying crystal structures and variations in atomic spacing. It is based on constructive interference of monochromatic X-rays when passing through a crystalline sample. The interaction of the incident rays with the sample produces constructive interference (and a diffracted ray) when conditions satisfy Bragg's Law ($n\lambda=2d \sin \theta$) (Fig.11). This law relates the wavelength of electromagnetic radiation to the diffraction angle and the lattice spacing in a crystalline sample. These diffracted X-rays are then detected, counted and processed. By scanning the sample through a range of 2θ angles, all possible diffraction directions of the lattice should be attained due to the random orientation of the powdered material. Conversion of the diffraction peaks to d-spacing allows identification of the mineral because each mineral has a set of unique d-spacing. Typically, this is achieved by comparisons of the obtained d-spacing information with the standard reference patterns.

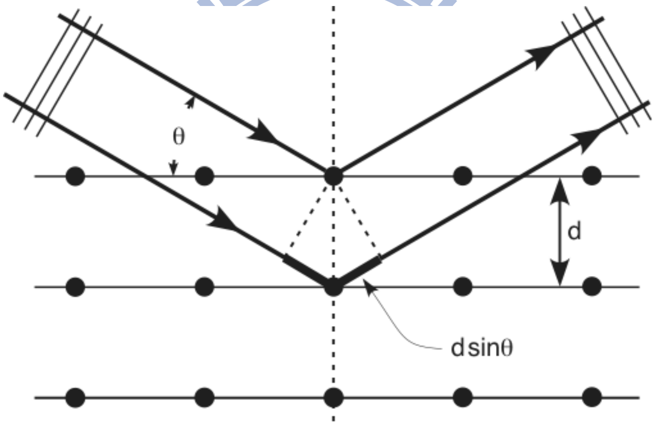

Fig. 11 The illustration of XRD process.

(II) X-ray Photoelectron Spectroscopy (XPS)

X-ray photoelectron spectroscopy (XPS), also called electron spectroscopy for chemical analysis (ESCA), is a popular surface analytic technique. It can provide detailed information about the elemental composition, chemical state and electronic structure of the elements that exist within a material [66-68]. XPS is based on the photoelectric effect, whereby a sample surface emit electrons after being irradiated by a photon source of sufficiently high energy, as shown in Fig.12 . For XPS, a soft x-ray

(50 — 1500 eV) are used as the exciting photon source. The surface atoms emit electrons (called photoelectron) after direct transfer of energy from the photon to the core-level electron, as illustrated in Fig. 13. The emitted electron is called *photoelectron* and the emitting process is named *photoemission*. The photoelectrons are subsequently separated according to their energy via an electron spectrometer.

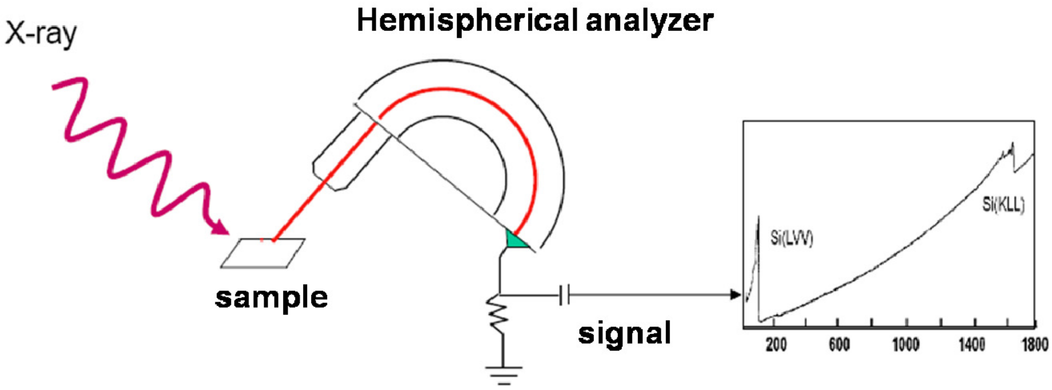

Fig. 12 Illustration of photoelectric effect

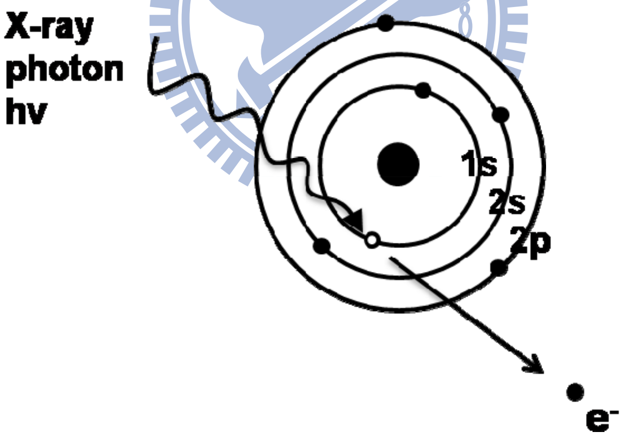

Fig. 13 The X-ray photon transfers its energy to a core-level electron imparting enough energy for the electron to leave the atom

Because the energy of a particular x-ray wavelength equals a known value, we can determine the electron binding energy of each of the emitted electrons by using an equation that is based on the work of Ernest Rutherford:

$$\mathrm{E_{binding}} = \mathrm{E_{photon}} - \mathrm{E_{kinetic}} - \Phi$$

where E_{binding} is the energy of the electron emitted from one electron configuration within the atom, E_{photon} is the energy of the x-ray photons being used, E_{kinetic} is the kinetic energy of the emitting electron as measured by the instrument and Φ is the work function of the spectrometer (not the material).

Core level peaks can provide direct information on the chemical bonding by XPS measurement. The characteristic binding energies of photoelectrons are not only element specific, but also depend on the chemical state of the corresponding atom. Chemical shifts are recorded as a displacement (typically in the range of 0 to 4 eV) in binding energies of photoelectrons excited from atoms in a compound compared to the energies of the corresponding pure substance. Binding energies increase, e.g., with the oxidation state of a substance, as part of the electronic density is transferred to the oxidizing species, leaving the remaining electronic density unbalanced against the positive nuclear charge.

(III) Superconducting Quantum Interference Device (SQUID)

A superconducting quantum interference device (SQUID) is equipment used to measure extremely weak signals, such as subtle the magnetic field changes in living organisms. SQUID is designed by use of the principal of macroscopic long-range quantum interference and consists of two parallel Josephson junctions made of two superconductors separated by a thin insulating layer. The device may be configured as a magnetometer to detect incredibly small magnetic fields. The great sensitivity of the SQUID devices is associated with measuring changes in magnetic field associated with one flux quantum. One of the discoveries associated with Josephson junctions were the flux is quantized in units. If a constant biasing current is maintained in the SQUID device, the measured voltage oscillates with the changes in phase at the two junctions, which depends upon the change in the magnetic flux. Recording the oscillations allows us to evaluate the flux change which has occurred. Hence, SQUID as magnetometer provides the information of magnetic field gradient or magnetic field of sample.

(IV) Electron Paramagnetic Resonance (EPR)

Electron Paramagnetic Resonance (EPR) often called Electron Spin Resonance (ESR) is a branch of spectroscopy in which electromagnetic radiation (usually of microwave frequency) is absorbed by molecules, ions or atoms possessing electrons with unpaired spins.

Ever since the discovery of Electron Paramagnetic Resonance by

Zavoiskii, it has been developed into an important branch of spectroscopy and becomes a valuable tool in all branches of science wherever systems containing unpaired electrons are investigated.

Intrinsic spin is a unique quantum property of electron, nuclei, and nuclear and sub nuclear particles. Charged particles with spin or orbital angular momentum will have magnetic moments, a vector quantity denoted as such by the bold character μ. The magnetic moment μ interacts with the static vector magnetic field B to produce an energy U through the following scalar product relationship.

$$U = -\mu \cdot B$$

This component of the electron energy is designated as the Zeeman interaction. Static magnetic field generates an energy-level structure. Magnetic fields that vary rapidly with time stimulate transitions between energy-levels or states, giving rise to spectral lines. Energy states are quantitatively called the spin Hamiltonian. From the Hamiltonian, the energy level structure can be derived. The intrinsic spin gives the electron its intrinsic spin magnetic charge will create a current loop. An electron can have angular momentum as it moves not only around its own axis but also in an orbit.

The component μ_z of electron-spin magnetic moment along the direction of the magnetic field B applied along the direction z is

$$\mu_z = -g_e\beta_e M_s \ ; \ \beta_e = \frac{|q|\hbar}{2m}$$

where g is the Zeeman factor. This was originally introduced to correct and increase, by a factor of 2, the relationship between magnetic moment and spin from what would be expected from the relationship between magnetic moment and orbital angular momentum.

For a single unpaired electron, the possible values of M_s are $+\frac{1}{2}$ and $-\frac{1}{2}$. Hence the possible values of μ_e are $\mp\frac{1}{2}g_e\beta_e$ and the values of U are $\pm\frac{1}{2}g_e\beta_e B$ (Fig. 14). These are sometimes referred to as the electronic Zeeman energy.

$$\Delta U = g_e\beta_e B$$

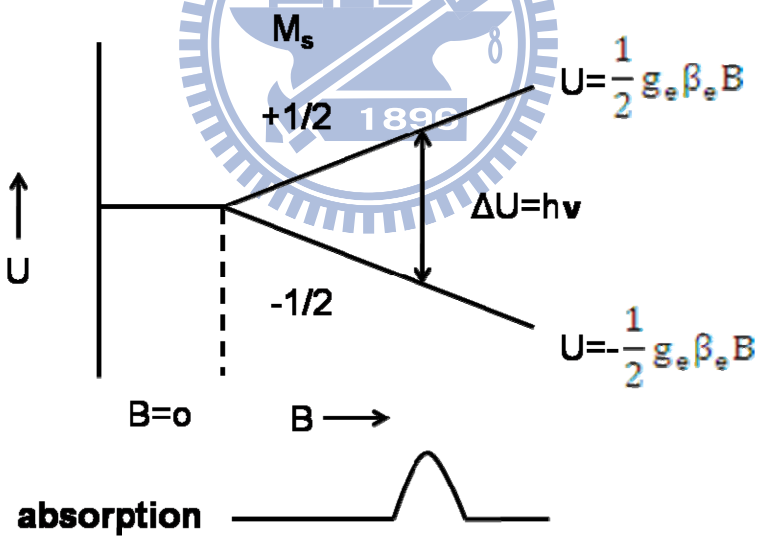

Fig. 14 Energy-level scheme for the simplest system (e.g., free electron) as a function of applied magnetic field B, showing EPR absorption.

By placing the unpaired electrons in a magnetic field, we have increased the number of energy levels from one to two. In fact, sometimes in the region near the electron there is an atomic nucleus with a magnetic moment. The magnetic moment of the nucleus is restricted to a few orientations with respect to an external magnetic field. The magnetic energy of the electron is affected by the orientation of the nuclear magnetic moment. It is the reason why two magnetic energy levels for the electron are each further split into a few sublevels. This interaction of the nucleus and the electron is called the hyperfine interaction.

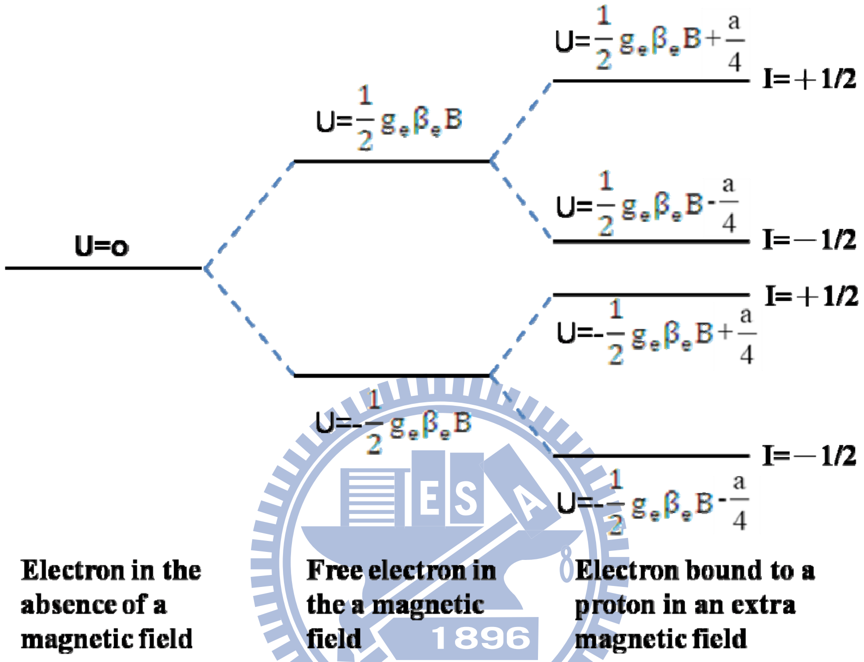

Fig. 15 Hyperfine splitting in the hydrogen atom in a high field.

The applied magnetic field splits the energy levels in to $M_s = +\frac{1}{2}$ and $-\frac{1}{2}$ states. Each M_s state splits into two M_I states due to interaction with He nucleus ($I=\frac{1}{2}$). We observe transitions between levels 4 and 1, 3 and 2. Therefore the “selection rules” for EPR transitions are $\Delta M_s = \pm 1, \Delta M_I = 0$. The proton has a spin of $\frac{1}{2}$. By the 2I+1 rule, the number of possible orientations is two. The number of levels is produced by hyperfine splitting. That is the reason there will be four levels. The Hamiltonian for the magnetic interaction in a strong external field is

$$K_{magnetic} = g\mu_0 H_z S_z + aI_zS_z$$

By using the Hamiltonian we find that the energy in the state $| M_s M_I \rangle$ is

$$U(M_s M_I) = g\mu_0 H_z M_s + a M_s M_I$$

Most of the electrons in atoms, molecules, and solids do not give EPR signals. Due to electrons are not unpaired in these substances. This means that for every electron in the $M_s = -\frac{1}{2}$ state there is another electron in the same orbital and in the $M_s = \frac{1}{2}$. Transition from the $-\frac{1}{2}$ state to the $\frac{1}{2}$ state would put two electrons in the same orbital and the same spin state. Unpaired electrons of substance are called paramagnetic substances which include organic free radicals, transition metal ions, metals, crystals with certain defects.

EPR experiments manipulate a Bruker spectrometer at X-band (ν=9 GHz). DPPH was used as a reference for calibration of g factors. The shape and the area of the EPR spectra were analyzed by standard numerical methods.

Chapter 4

Results and discussion

4-1 Nitrogen-doped Titanium Dioxide

(I) XRD

N-doped TiO_2 powder prepared by annealing the TiO_2 powder at various nitrogen pressures is evidenced by XRD θ-2θ scans shown in Fig. 16. The XRD pattern for pure TiO_2 without the treatment is also included for comparison. All samples are single phase (rutile) with no evidence of secondary phase within the XRD measurements. Therefore, the possibility of the contribution of ferromagnetism from the secondary phase can be excluded. In addition, a color change in the TiO_2 powders from white to black was noticed after treatment. It is called F-center which is a type of crystallographic defect in which an anion vacancy in a crystal is filled by one or more electrons, depending on the charge of the missing ion in the crystal. Electron in such a vacancy tends to absorb light in the visible spectrum such that the originally transparent material becomes colored [69, 70].

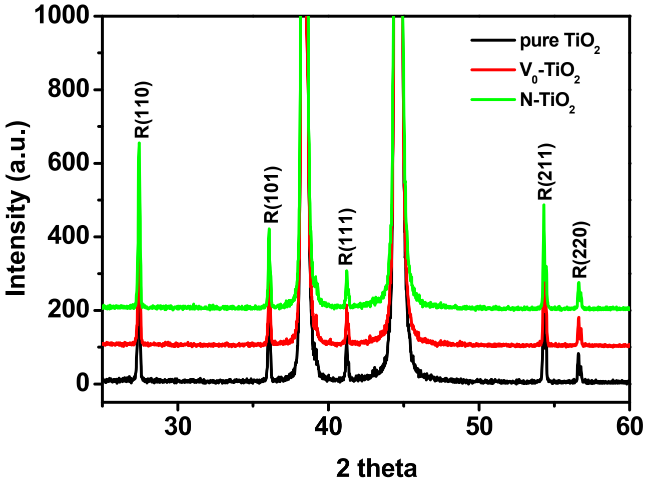

Fig. 16 XRD patterns of samples pure TiO_2, V_0-TiO_2, and N-TiO_2.

(II) SQUID

Fig. 17(a) shows the magnetization (M) versus field (H) curves taken at 300K for pure TiO_2 (rutile), V_0-TiO_2, and N-TiO_2 powders. From the partial hysteresis loop shown in Fig. 17(b), it is evident that pure TiO_2 is completely paramagnetic, while V_0-TiO_2 is predominantly paramagnetic with minute sign of ferromagnetism. On the contrary, the N-TiO_2 exhibits marked ferromagnetic feature at room temperature. The magnetic parameters for V_0-TiO_2 are estimated to have 6×10^{-6} emu/g for remnant magnetization and 35.7 Oe for coercive force, respectively. The slight ferromagnetism is believed to arise from the contribution of oxygen vacancies introduced by heating the TiO_2 powders at high temperature in vacuum. Coey et al. [71] proposed that the ferromagnetism is originating from direct exchange interaction between the molecular orbital consisting of the valence electrons of the three titanium ions and the oxygen vacancy surrounded by them. The molecular orbital results in ferromagnetism when the concentration of oxygen vacancies, namely, the concentration of molecular orbital, is large enough. However, if the concentration of oxygen vacancies is low, the isolated molecular orbital will result in paramagnetism. This model is similar to that described by the BMP model. In the BMP scenario, oxygen vacancies act both as electron donors and electron traps which can bind the electron, and then combining with the three titanium ions in the vicinity to form a bound magnetic polaron. In Coey's case, it is named as molecular orbital. If neighboring BMPs do not interact strongly with each other, a paramagnetic, insulating phase results. However, for certain BMP–BMP distances and combinations of electron–electron and electron–local moment exchange constants, the BMPs may couple in a ferromagnetic fashion.

On the other hand, when nitrogen is introduced by high temperature annealing, it is clear from Fig. 17(b), an obvious M-H hysteresis loop representing the existence of ferromagnetism is seen. From the hysteresis loop, we estimate a saturation magnetization (Ms) of 9×10^{-4} emu/g, a remnant magnetization of 7×10^{-5} emu/g, and a coercive force of 74.1 Oe for sample N-TiO_2, respectively. Those values are apparently orders of magnitude larger than those obtained for V_0-TiO_2, indicating a much stronger ferromagnetic characteristic. Based on the density functional theory (DFT) calculation by Di Valentin et al. [72], it has been shown that a large decrease in the formation energy of oxygen vacancies can be gained owing to the presence of nitrogen atoms in the lattice. It also suggests that oxygen vacancies are most probably induced by N-doping of TiO_2. We will confirm this assertion by XPS in the next section. In any case, all of these arguments imply that TiO_2 powders will lose more oxygen or have more oxygen vacancies when doped with nitrogen and, more importantly, it also induces strong ferromagnetism. However, it is not clear whether the stronger ferromagnetism is correlated solely to the larger concentration of oxygen vacancies or something else.

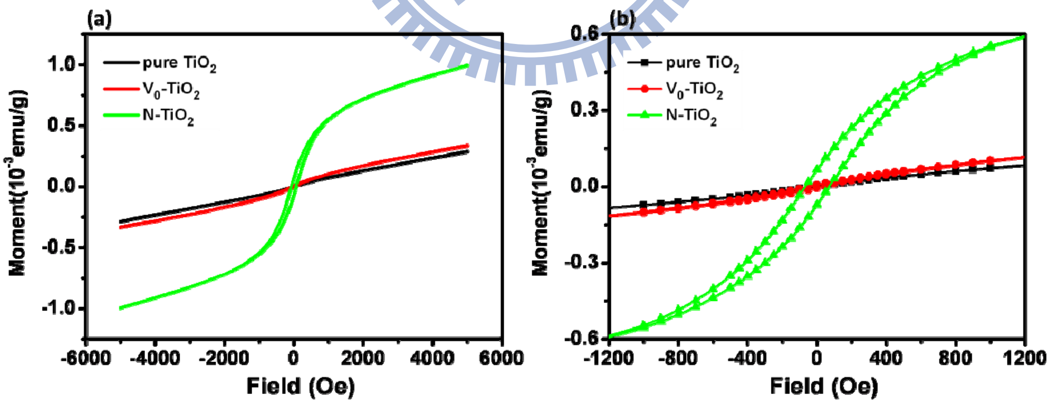

Fig. 17 (a). Magnetization versus magnetic field (M-H) at 300K for V_0-TiO_2 and N-TiO_2. (b) The partial hysteresis for all samples.

Alternatively, Shen et al. [53] proposed p-p coupling interaction for ferromagnetism in N-doped ZnO. It was believed that substitution of nitrogen atoms at oxygen sites in ZnO introduces holes in O 2p states, which couple with the parent

N 2p localized spin via the p-p interaction, similar to p-d hybridation in TM-doped DMS. This interaction follows essentially from quantum-mechanical level repulsion, which "pushes" the minority states upward, crossing the Fermi-level. A strong p-p coupling interaction between the impurity state and valence-band state is allowed near the Fermi-level. In other words, nitrogen-doping induces interaction between the impurity state and valence-band state so that the minority states cross the Fermi-level. It effectively has similar results as the Stoner splitting both induces extra states near the Fermi-level. Consequently, if it satisfies the Stoner criterion it would promote spontaneous ferromagnetism. As will be described later, the valence band XPS indeed indicates that there are extra states near the Fermi-level in N-doped TiO_2. Briefly, we have found that nitrogen-doping not only creates more oxygen vacancies but also introduces p-p interaction between the N 2p and O 2p. Both factors are probably working together to result in the significant room-temperature ferromagnetism observed in N-TiO_2.

(III) XPS

As mentioned above, the XPS spectra may provide crucial information for clarifying the effect of nitrogen dopant and oxygen vacancies on the very different M-H results observed in TiO_2 treated under various conditions. In Fig. 18, all the peaks reported were charge corrected using C 1s peak position at 284.5eV as the reference point. Fig. 18(a) shows the high-resolution O 1s XPS spectra of all samples and Fig. 18(b. I, II) is the fitting results for the pure TiO_2 and the N-doped TiO_2 samples, respectively. From Fig. 18(b. II), the peak can be divided into three symmetric peaks. The origin of the peak at the lowest binding energy (peak 1) is not clear. For the medium binding energy (peak 2), it is ascribed to the O 1s core peak of O^{2-} bound to Ti^{4+}. Perhaps, the most prominent peak is peak 3 with the highest binding energy, which is referred to as the high binding energy component (HBEC) and the peak 2 is referred to as the low binding energy component (LBEC) [73]. It has been previously reported that the HBEC component develops with the increasing loss of oxygen [74]. Furthermore, the relative area under the curve (area of HBEC peak/area of LBEC peak) is determined to be 0.369 for pure TiO_2, 0.387 for V_0-TiO_2, and 0.680 for N-TiO_2, respectively. The relatively large contribution of the HBEC peak for the case of annealing in nitrogen gas strongly suggests the presence of nitrogen may have introduced more oxygen vacancies in our case (Fig.19). This may be also relevant to the obvious M-H curve hysteresis loop observed for the N-TiO_2 sample. At this stage, it appears that oxygen vacancies may have played an important role in the origin of ferromagnetism of doped TiO_2.

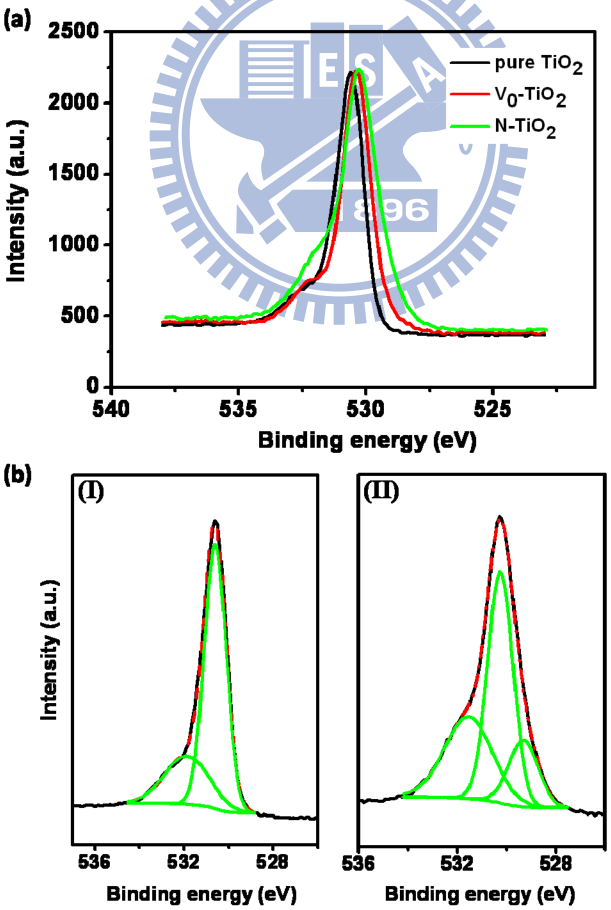

Fig. 18 (a) XPS spectra of O 1s core level for pure TiO_2, V_0-TiO_2, and N-TiO_2 samples. (b) Fitting results of O 1s XPS spectra for (I) pure TiO_2 and (II) N-TiO_2

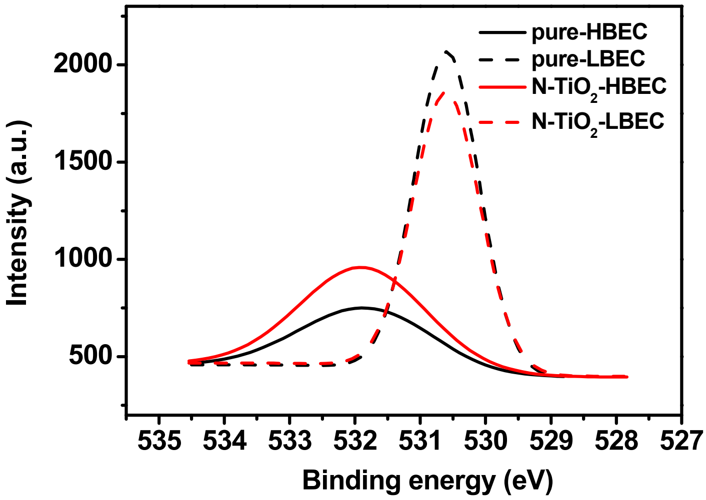

Fig. 19 HBEC peak and LBEC peak in pure TiO_2 and N-TiO_2 samples.

In order to further clarify the role played by nitrogen, we have also investigated the XPS of Ti ions. From Fig. 20(a), the high-resolution Ti 2p XPS spectra evidently show that, pure TiO_2 only has Ti^{4+} signal with characteristic $2p_{3/2}$ and $2p_{1/2}$ spin doublet at 459.3 eV and 465.2 eV, respectively, corresponding to a peak separation of 5.9 eV. Ti^{4+} is non-magnetic in stoichometric TiO_2, since it does not have any unpaired 3d electron. However, unpaired 3d electron in Ti^{3+} or Ti^{2+} can lead to some magnetic moment. It is known that oxygen vacancies may change the charge balance and therefore there is a possibility to generate Ti^{3+} or Ti^{2+}. In Fig. 20(b) we can observe clearly the difference between N-doped TiO_2 and pure TiO_2. Therefore, we can fit the extra spectra appeared in N-TiO_2 and try to understand these. From Fig. 20(b), in addition to the above mention peaks, there are extra peaks labeled as peak 3 and peak 4. These two peaks might correspond to $2p_{3/2}$ and $2p_{1/2}$ of Ti^{3+} or Ti^{2+}. The slightly lower binding energy for peak 3 suggests that the removal of oxygen may lead to a higher electron cloud density than in the case of Ti^{4+}. However, at present, we are unable to identify the exact valence of the Ti ions, albeit that a reduction is evident. In any case, the features for both the core level peaks of O 1s and Ti 2p strongly suggest the existence of oxygen vacancies.

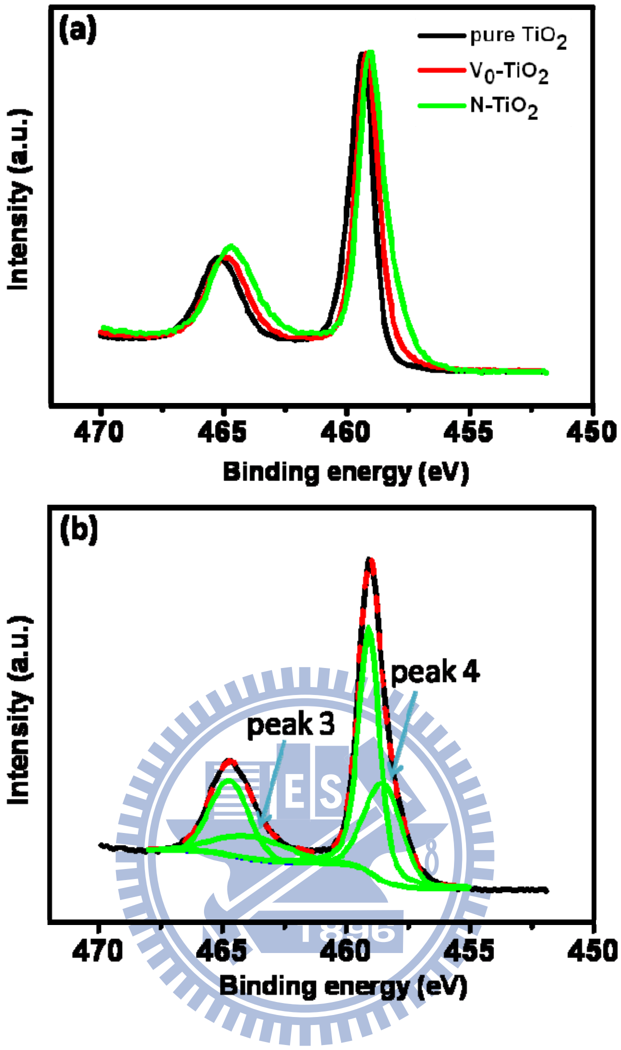

Fig. 20 (a) XPS spectra of Ti 2p core level for pure TiO_2, V_0-TiO_2, and N-TiO_2samples. (b) Fitting result of Ti 2p XPS spectra for N-TiO_2samples.

Next, we turn to discuss the effect on N-doping on the density of states (DOS) near the Fermi-level. The XPS spectra of valence band for all samples are shown in Fig. 21. Curves are plotted by setting the Fermi-level to be equal to zero. For one thing, we can observe slight state appeared near the Fermi-level in sample V_0-TiO_2. On the other hands, it is clear that there exists marked difference in the DOS near the Fermi-level between N-doped TiO_2 and the rest of the samples. Pure TiO_2 has primarily a filled O 2p derived valence band separated from an empty Ti 3d, 4s and 4p derived conduction band by a bulk band-gap of 3.2 eV [75]. The valence band spectra show the emission from O 2p band with its upper edge lying 3 eV away from the Fermi-level. It has been pointed out that the feature close to 0 eV in the reduced TiO_2 or anion-doped TiO_2 can be attributed to the occupied defect states (or impurity state) corresponding to the partial population of Ti 3d band [76]. Thus, in our case, the doping of nitrogen into TiO_2 must have somehow induced significant amount of oxygen vacancies, as reflected in the significant growth of the occupied-defect states related feature near the Fermi-level. This is also consistent with the first-principle calculation by Rumaiz [55], wherein it was shown that N doping in TiO_2 leads to the formation of oxygen vacancies. It appears that the observed occupied states of Ti-3d near the Fermi-level and the modification of electronic structure are intimately related not only the doped N-impurities but also the oxygen vacancies.

Furthermore, Fig. 21 also shows that the O 2p valence band is shifting to lower binding energy with nitrogen doping. It is suggestive that the incorporation of less tightly bound N 2p level with O 2p level further cause slight band-gap shrinkage. Alternatively, it may also relate to the p-p interaction between the impurity p states (N 2p) and the host p states (O 2p) at the top of the valence band. Though this interaction, the Stoner splitting might be induced to promote the ferromagnetism given by the Stoner criterion. The simultaneous presence of the nitrogen dopants and oxygen vacancies, in addition to result in the formation of new states near the Fermi-level, may push the system all the way to surpass the Stoner criterion. If we denote the density of states at the Fermi-level as $g(\varepsilon_f)$ and U as the Coulomb energy, the condition for spontaneous ferromagnetism given by the Stoner criterion is $U\, g(\varepsilon_f) \geqq 1$. Thus, it should be interesting to see if our system is in the conditions of leading to Stoner splitting of the band and then induce ferromagnetism.

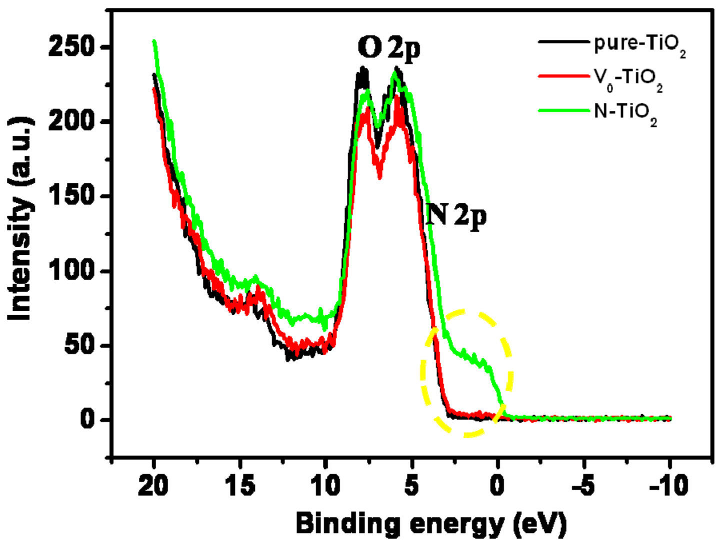

Fig. 21 Valence band XPS spectra for pure TiO_2, V_0-TiO_2, and N-TiO_2 samples.

This exchange splitting of the conduction band can be observed in Fig. 22, where the binding energy shift is attributed to a chemical potential shift. Fig. 22 shows Ti 2p and O 1s core level spectra for pure TiO_2, V_0-TiO_2 and N-TiO_2. We can observe that the core peaks of both O 1s and Ti 2p are shifted to lower binding energy. The fact that the N-TiO_2 sample has the most binding energy shift among all samples is most likely due to the Stoner splitting [77]. This also explains the marked enhancement of ferromagnetism displayed in the M-H hysteresis for the N-TiO_2 sample.

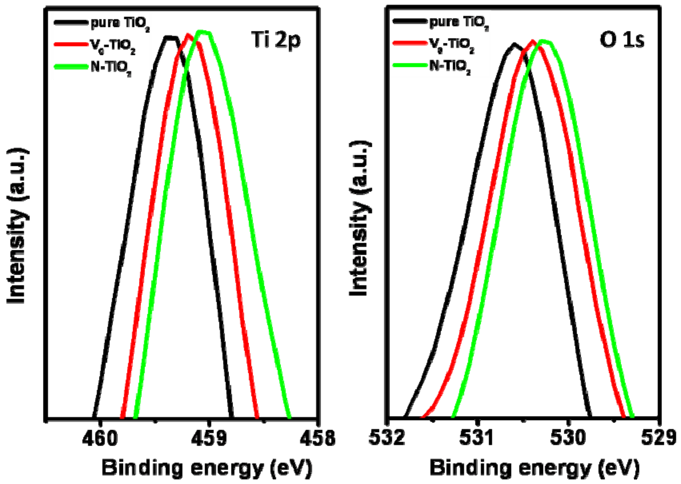

Fig. 22 O 1s and Ti 2p core level peaks for all samples showing the chemical potential shift

In short, in this section, we have shown that nitrogen doping in TiO_2 generates oxygen vacancies and new states near the Fermi-level simultaneously, such that pushes the system all the way to surpass the Stoner criterion for inducing the Stoner exchange splitting of the band and lead to ferromagnetism.

(IV) EPR

The next question to be asked is how the N-doping cope with the oxygen vacancies to give rise to the observed phenomena? To probe the exact electronic configuration and to gain more insight about the mechanism of the ferromagnetism in the N-TiO_2 sample, EPR measurements were carried out. It is an effective tool to investigate the origin and nature of observed ferromagnetism in a material, in particular, to extract information about the oxidation state of the dopant cation involved in the spin coupling.

For the electron structure of N doped TiO_2, Di Valentin et al. [78] have proposed two models in their DFT calculations. In substitutional model, nitrogen atom is assumed to replace oxygen in TiO_2, so that nitrogen atom accepts the extra charge from oxygen atom and is in the state of negative oxidation. On the other hand, in the interstitial model, the nitrogen atom is assumed to bind with one lattice oxygen to form a NO species. These species, then, interact with the Ti atoms through their π bounding state in TiO_2. In either case, however, the unpaired electrons are almost localized on the surrounding of nitrogen atoms.

On the contrary, it was shown experimentally [78,79] that most of the unpaired electrons do not distribute in the vicinity of nitrogen atom based on the observations of the EPR signals which gave g values of 1.99-1.93 attributable to the Ti^{3+} species. Fig. 23 reveals the presence of active species trapped on Ti^{3+} site (1.94) in V_0-TiO_2 sample, which appears to be consistent with the previous results. Nevertheless, on the right hand side of the Ti^{3+} signal for N-TiO_2 sample, the position apparently shifts by 0.02 to higher magnetic field. The line width (ΔH_{pp}) of V_0-TiO_2 and N-TiO_2 is 70G and 170 G, respectively. There are not any EPR signals in pure TiO_2. It conforms that the removal of oxygen will lead to a higher electron cloud density than that of intrinsic Ti^{4+}, so that the valence of Ti is effectively decreased. However, by comparing with the M-H loop results, the sample V_0-TiO_2 does not appear to possess obvious ferromagnetism even though the Ti^{3+} species are already existent. Hence, we speculate that Ti^{3+} alone may not be the primary factor for ferromagnetism.

Thus, there must be something else involved in giving rise to the significant ferromagnetism seen in N-TiO_2 sample. It is noted that the line width of N-TiO_2 extends to lower magnetic field and higher magnetic field for the left-hand side and the right-hand side EPR peak, respectively, as compare to that of the V_0-TiO_2 sample (Fig. 23). We believe that this is due to the supposition of other overlapping signals, presumably originated from the nitrogen impurities. Since the EPR signals for N-centers are having g-values between 2.003-2.005 [78, 79]. This broad signal is attributed to ferromagnetic resonance (FMR) arising from exchange interaction between BMPs. The fact that both V_0-TiO_2 and N-TiO_2 exhibit the existence of the Ti^{3+} signal but only N-TiO_2 showed ferromagnetism, further implies that the combination of nitrogen and the associated increasing in oxygen vacancies is the key to induce ferromagnetism.

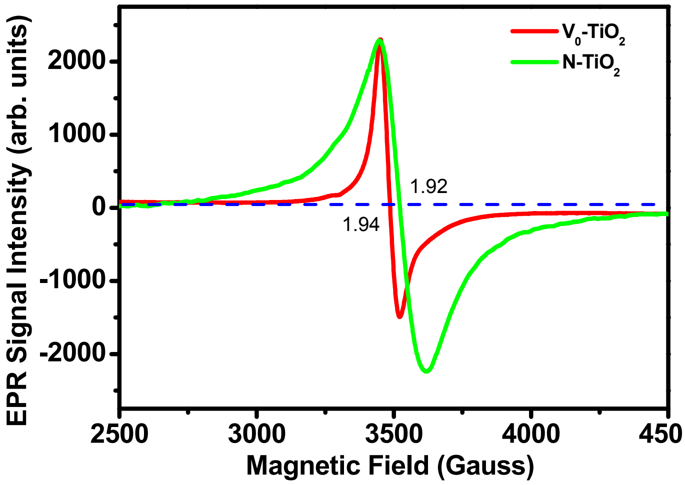

Fig. 23 EPR spectra of V_0-TiO_2 and N-TiO_2 samples.

(V) Summary

In summary, standard DMSs usually dope transition elements which possess unpaired d or f electron in materials. However, the standard theories for explaining DMSs are found inapplicable to the newly discovered 2p-light elements doped materials. There are several important differences between the 2p and 3d orbital which determine the different magnetic properties exhibited in DMSs doped with 2p LE (anion) and 3d TM (cation). First, the anion 2p bands of the element are usually full in ionic states, leaving no room for unpaired spins compared to 3d bands for transition metal. Second, p states are inefficient in the spin-orbital interaction compared to d states. Third, valence electrons in p states are more delocalized than those in d- or f- states. It means that they have much larger spatial extension which can facilitate long-range exchange coupling interactions. Therefore, 2p light-element doped DMSs can have weak ferromagnetism even with low doping concentration.

Consequently, 2p light elements are appropriate candidate for dopant in DMSs that are able to induce room temperature ferromagnetism. In our experiment, nitrogen doping promotes the formation of excessive oxygen vacancies, as indicated by the marked enhancement of HBEC component in the XPS results. From the valence band XPS spectra (Fig. 22), it is evident that the O 2p valence band moves to lower binding energy with nitrogen doping due to the engagement of p-p interaction. In other words, doping nitrogen into TiO_2 not only induces the formation of oxygen vacancies but also activates the p-p interaction between the impurity state (N 2p) and valence band state (O 2p). This interaction pushes the minority states upward, crossing the Fermi-level and triggers the Stoner splitting to extend the tail of the valence-band maximum to lower binding energy and produces extra states below the maximum as compared to undoped TiO_2. It not only satisfies the Stoner criterion but also creates unpaired electrons when charge transfer happens so as to promote spontaneous ferromagnetism. The unpaired electrons originated from the interaction between impurities and the lattice oxygen in TiO_2 manifests itself by the broad signal associated with the ferromagnetic resonance in EPR spectra. It acts as spin-polarized carrier sources.

Within the context of current scenario, the combined effects of the p-p coupling interaction and charge transfer near each impurity will tend to align spins and form moment carried by the impurity ion. The moment carrying impurities then couples strongly with carrier spin generated by oxygen vacancies to form long range BMPs. The primary reason is due to the spatially-extended p-states inherent to the impurities are able to facilitate long-range magnetic coupling. If the concentration of BMPs is sufficiently high, it is able to effectively mediate indirect ferromagnetic coupling among impurities by carriers. Finally, not only spin of impurities but also carrier spins are aligned to result in ferromagnetism (Fig. 24). This model gives a reasonable explanation to the experimentally observe ferromagnetism in TiO_2 doped with small amount of nitrogen.

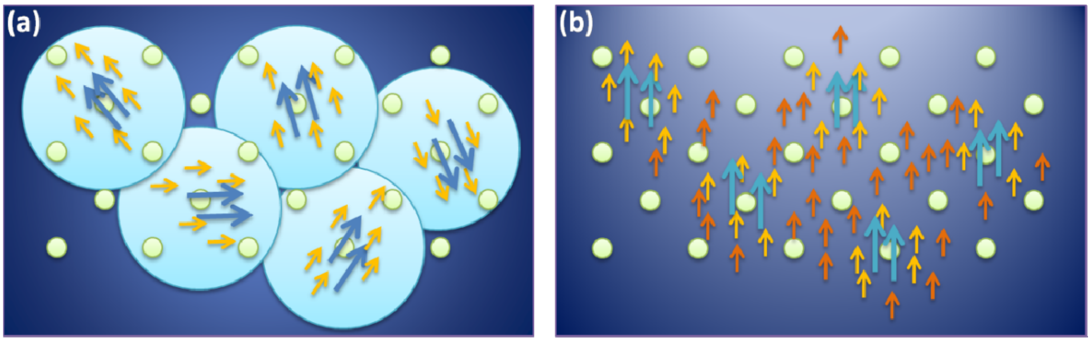

Fig. 24 Schematic showing ferromagnetic coupling between impurities. (a) The magnetic moment of impurities polarizes carriers and aligns the spins of the carriers in the same direction as BMP. (b) If the carrier concentration is sufficiently high, it is able to effectively mediate indirect ferromagnetic coupling among nearly all BMP. Cation is not shown in the diagram.

4-2 Carbon-doped Titanium Dioxide

(I) XRD

The crystal phase of the pure TiO_2 with carbon is identified by a conventional XRD shown in Fig. 25. The results in C-mixed TiO_2 (no annealing) and C-doped TiO_2 (annealing) powders are transparent suggesting that both samples are of homogenous rutile phase. The only difference is the carbon signal. The signal of carbon of the C-doped TiO_2 sample decreases significantly after annealing. We believe that most carbon reacted with TiO_2, rather than just burned out, because the base pressure was kept under 6×10^{-4} torr during the entire process. Moreover, since there is no titanium carbide phase discernible from the XRD results, the carbon must have substituted oxygen or got into the interstitial sites of TiO_2. In order to check the assertion described above, we utilize XPS to investigate the existence of carbon in TiO_2.

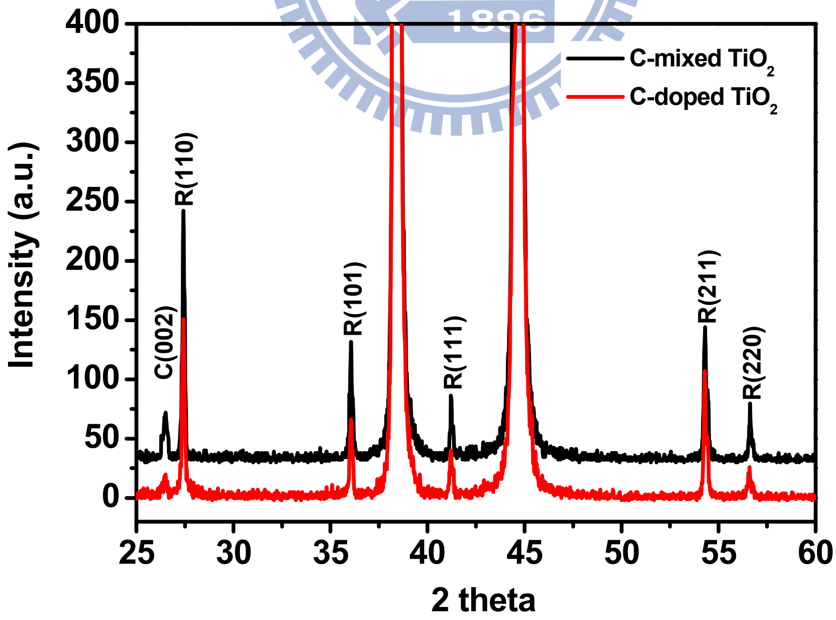

Fig. 25 XRD patterns of samples C-mixed TiO_2 and C-doped TiO_2.

(II) XPS

Fig. 26 shows the C 1s XPS profiles. We can observe that the C 1s spectra stretch over a broad energy range from 280 to 291 eV, which can be well fitted to five peaks. The peak 1 (288.8 eV) and peak 2 (286.3 eV) are attributed to carbonate species, and peak 3 (285.3 eV) is assigned to contaminated hydrocarbons [81]. The peak 4 (284.5 eV) is assigned to the active carbon from carbonic ink or adventitious carbon contamination adsorbed from the atmosphere. Hashimoto et al. [82] observed C 1s XPS peak at 282 eV (peak 5) and they assigned this C 1s XPS peak to Ti-C bond in carbon-doped TiO_2. Since the peak at 282 eV was observed for the carbon-doped TiO_2 powder and the corresponding XRD results did not indicate the existence of a TiC phase, thus, it is natural to attribute the Ti-C bond related peak to the substitution of carbon on the oxygen sites.

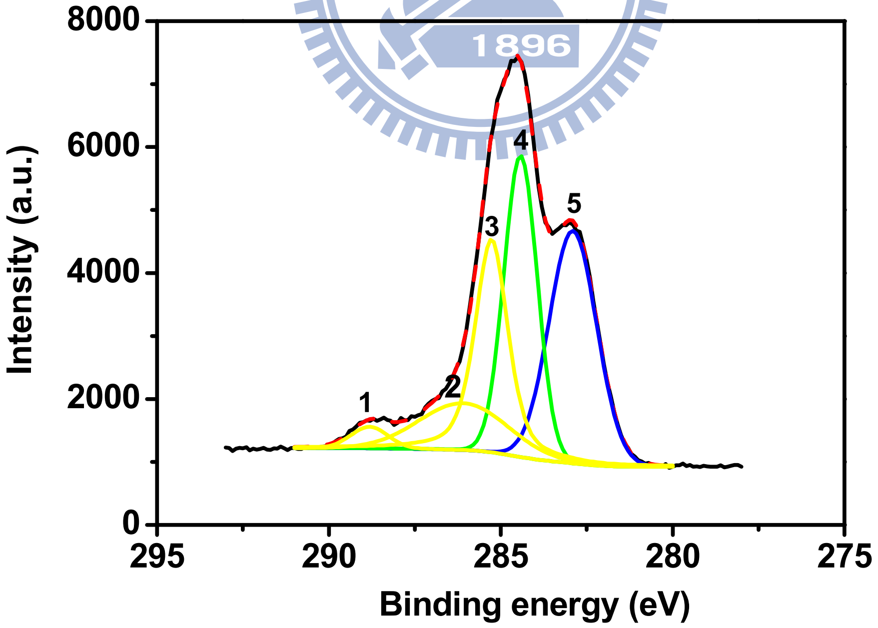

Fig. 26 Fitting result of C 1s XPS spectra for C-doped TiO_2 samples.

On the other hand, the high-resolution Ti 2p XPS spectra shown in Fig. 27 indicate that C-doped TiO_2 is similar to N-doped TiO_2. Namely, it exhibits not only the signature of the Ti^{4+} species but also the peaks with slightly lower binding energies (peak 3, 4). Again, it suggests that C-doped TiO_2 may also introduce excessive oxygen vacancies as that seen in N-doped TiO_2. The primary difference between N-doped TiO_2 and C-doped TiO_2 is that there exists extra peak (peak 5) in Ti 2p XPS spectra of the latter. We conjecture that peak 5 is derived uniquely from the Ti-C bond [82]. Both features in the core level peaks of C 1s and Ti 2p strongly suggest that carbon substitutes some of the lattice oxygen atoms. Comparing the results for N-doped TiO_2 and C-doped TiO_2, the latter appears to have more substitution for lattice oxygen atoms, because of the large signals detected. As a result, it might also introduce more oxygen vacancies in system. Fig. 28 shows the high-resolution O 1s XPS spectra. In that the relative area under the curve ((area of HBEC peak (peak 1) / area of LBEC peak (peak 2)) is determined to be 0.83 for C-doped TiO_2, 0.680 for N-doped TiO_2. It indicates that carbon substitution should be more favorable for the formation of oxygen vacancies in TiO_2 system. It is consistent with the observation [83] that both substitutional and interstitial C doping induces a strong reduction of the oxygen vacancy formation energy. Furthermore, more substitution also enhances the amount of the occupied impurity states near the Fermi-level. The valence band spectra that compare the results of C-TiO_2 and N-TiO_2 are shown in Fig. 29. We can observe that more prominent occupied impurity states near the Fermi-level in C-TiO_2 than in N-TiO_2, with the O 2p valence band moving to the lowest binding energy in C-TiO_2. Because more substitution of carbon for the lattice oxygen atoms can facilitate more incorporation with oxygen in the lattice by the p-p interaction, it might satisfy the Stoner criterion and induce the Stoner splitting and associated ferromagnetism. Indeed, as will be shown next, the magnetic properties probes by using SQUID evidently confirm the above assertions.

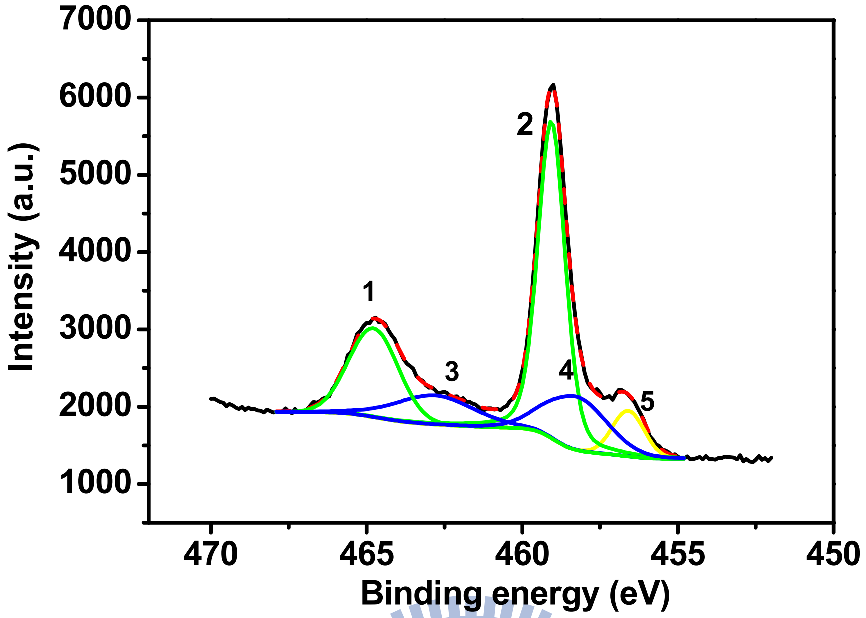

Fig. 27 Fitting result of Ti 2p XPS spectra for C-doped TiO_2samples.

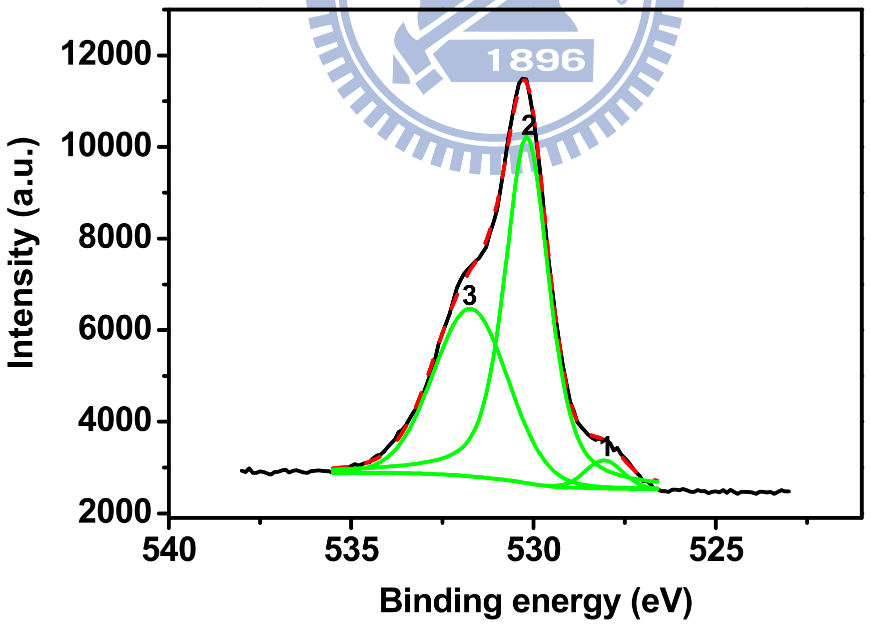

Fig. 28 Fitting result of O 1s XPS spectra for C-doped TiO_2samples.

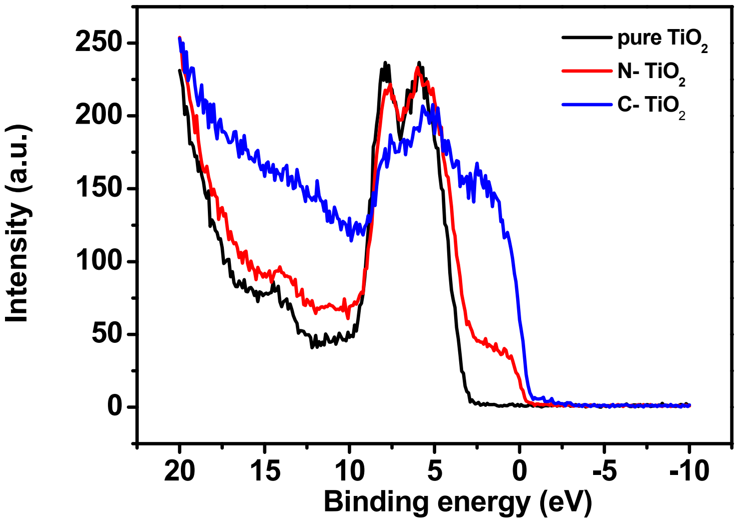

Fig. 29 Valence band XPS spectra for pure TiO$_2$, N-TiO$_2$, and C-TiO$_2$ samples.

(III) SQUID

The inset in Fig. 30 evidently demonstrates that pure TiO$_2$ is completely paramagnetic and, on the contrary, pure carbon is diamagnetic. Comparing the magnitude of slope between pure TiO$_2$ and carbon suggests that the diamagnetic moment of carbon is larger than the paramagnetic moment of pure TiO$_2$. Therefore, the diamagnetic moment and paramagnetic moment competes each other in the mixture of TiO$_2$ and carbon in magnetic field. Nevertheless, after the annealing process, something interesting has happened. First, if carbon and TiO$_2$ remained as a mixture after annealing, one would expect a linear superposition of the diamagnetic moment from carbon and paramagnetic moment from TiO$_2$ in the M-H curve. Second, if carbon had been burned out in vacuum without interacting with TiO$_2$, the diamagnetic moment would decrease dramatically and one would see predominantly only paramagnetic signal. Instead, none of these scenarios occurred. As displayed clearly in Fig. 30, the M-H curve taken at 300 K evidently exhibits significant room-temperature ferromagnetism in the current C-TiO_2 samples. From the partial hysteresis loop, we can estimate a saturation magnetization (Ms) of 0.64×10^{-3} emu/g, a remnant magnetization (Mr) of 0.13×10^{-3} emu/g, and a coercive force of 403.3 Oe, respectively. The much more pronounced ferromagnetism seen in C-TiO_2 than in N-TiO_2 are believed to arise from the more substitution for the lattice oxygen atoms mentioned above.

According to the features in XPS spectra and M-H curve, carbon atoms substitute oxygen atoms in carbon-doped TiO_2 system. That induces not only the formation of oxygen vacancies but also p-p interaction between the impurity state (C 2p) and valence-band state (O 2p). So that to form new state near Fermi-level by Stoner splitting, and then to promote spontaneous ferromagnetism. It confirms that C-doped TiO_2 may induce ferromagnetism where C atoms substitute O atoms, based on first-principle density function theory calculations [54].

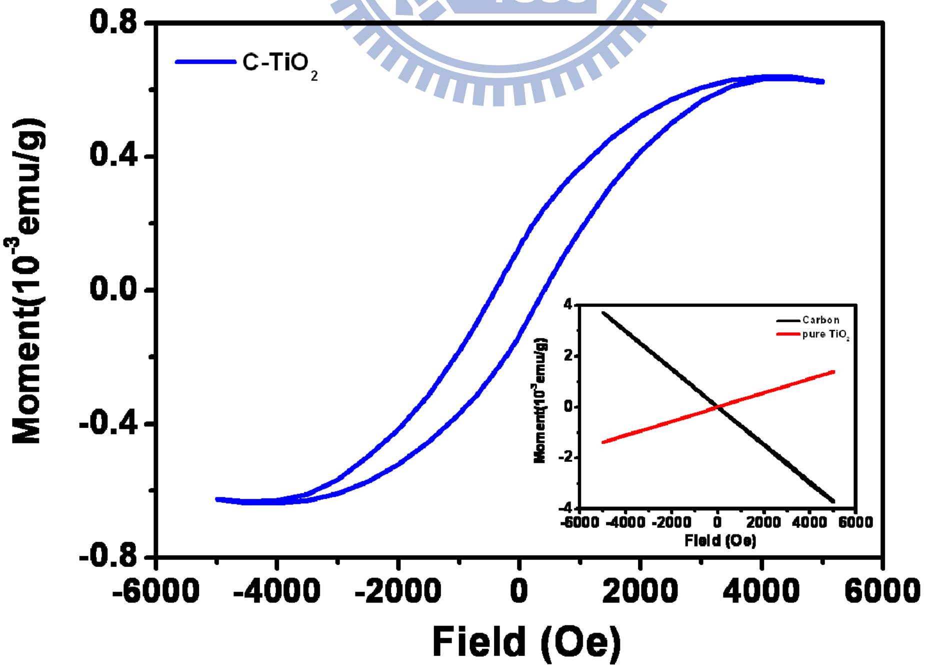

Fig. 30 Magnetization versus magnetic field at 300K for C-TiO_2. The inset shows magnetization of pure TiO_2 and carbon.

Chapter 5

Conclusion

In conclusion, we prepared nitrogen-doped TiO_2 and carbon-doped TiO_2 powders and investigated the ferromagnetic mechanism in qualitative.

1. From XRD measurements, all samples are of homogenous rutile phase so that there are no possibility of the contribution of ferromagnetism from the secondary phase can be excluded.
2. In the core level peaks of O 1s, the relatively large contribution of the HBEC peak for the case of 2p-light element doped TiO_2 strongly suggests the presence of impurities may have introduced more oxygen vacancies. It is known that the removal of oxygen may lead to a higher electron cloud density and therefore the extra peaks with slightly lower binding energies in Ti 2p XPS spectra. However, both features in the core level peaks of O 1s and Ti 2p strongly suggest the existence of oxygen vacancies.
3. The valence band can be able to evidence that the simultaneous presence of impurities and oxygen vacancies, in addition to result in the formation of new states near the Fermi level, may push the system all the way to surpass the Stoner criterion for inducing the Stoner exchange splitting of the band.
4. It not only satisfies the Stoner criterion but also creates unpaired electrons when charge transfer happens so as to promote spontaneous ferromagnetism. The unpaired electrons originated from the interaction between impurities and the lattice oxygen in TiO_2 manifests itself by the broad signal associated with the ferromagnetic resonance in EPR spectra.
5. The combined effects of the p-p coupling interaction and BMP model will

promote spontaneous ferromagnetism observed in 2p-light element doped TiO_2 from M-H curve

6. According to the features in XPS spectra strongly suggest that C-doped TiO_2 appears to have more substitution for lattice oxygen atoms. It might introduce more oxygen vacancies so as to enhance the amount of the occupied impurity states grown near the Fermi-level. Therefore, the much more pronounced ferromagnetism seen in C-TiO_2 than in N-TiO_2 are believed to arise from the more substitution for the lattice oxygen atoms mentioned above.

Our work demonstrates that nitrogen and carbon are novel impurities in the class of doped TiO_2 dilute magnetic semiconductor materials.

[1] 黃榮俊，自旋電子之研究與發展，物理雙月刊（廿六卷四期）(2008)

[2] 胡裕民, III-V稀磁性半導體薄膜之研究與發展，物理雙月刊（廿六卷四期）(2008)

[3] R. A. de Groot, F. M. Mueller, P. G. van Engen and K. H. J. Buschow, *Phys. Rev. Lett.* **50**, 2024 (1983)., *Phys. Rev. Lett.* **50**, 2024 (1983).

[4] S. M. Watts, S. Wirth, S. von Molnár, A. Barry and J. M. D. Coey, *Phys. Rev B* **61**, 9621 (2000).

[5] J.-H. Park, E. Vescovo, H.-J. Kim, C. Kwon, R. Ramesh and T. Venkatesan, *Nature* **392**, 794, (1998).

[6] J. J. Versluijs, M. A. Bari and J. M. D. Coey, *Phys. Rev. Lett*. **87**, 026601 (2001).

[7] K.-I. Kobayashi, T. Kimura, H. Sawada, K. Terakura and Y. Tokura, *Nature* **395**, 677 (1999).

[8] R P Borges, R M Thomas, C Cullinan, J M D Coey, R Suryanarayanan, L Ben-Dor, L Pinsard-Gaudart and A Revcolevschi, *J. Phys.: C M* **11**, L445 (1999).

[9] R. A. de Groot, F. M. Mueller, P. G. van Engen and K. H. J. Buschow, *Phys. Rev. Lett.* **50**, 2024 (1983)., *Phys. Rev. Lett.* **50**, 2024 (1983).

[10] T. Dietl, H. Ohno, F. Matsukura, J. Cibert and D. Ferrand, *Science* **287**, 1019 (2000).

[11] Sato K and Katayama-Yoshida H, *Japan. J. Appl. Phys.* **39** L555 (2000).

[12] Matsumoto Y, Murakami M, Shono T, Hasegawa T, Fukumara T, Kawasaki M, Ahmet P, Chikyow T, Koshihara S Y and Koinuma H, *Science* **291** 854 (2001).

[13] S. A. Chambers, T. Droubay, C. M. Wang, A. S. Leab, R. F. C. Farrow, L. Folks, V. Deline and S. Anders, *Appl. Phys. Lett.* **82**, 1257 (2003).

[14] A. Punnoose, M. S. Seehra, W. K. Park and J. S. Mooera, *J. Appl. Phys.* **93**, 7867 (2003).

[15] R. J. Kennedy and P. A. Stampe Erhong Hu, Peng Xiong and Stephan von Molna and Yan Xin, *Appl Phys. Lett.* **84**, 2832 (2004).

[16] R. Q. Wu, G. W. Peng, L. Liu1, Y. P. Feng, Z. G. Huang and Q. Y. Wu, *Appl. Phys. Lett.* **89**, 062505 (2006).

[17] L. H. Ye, A. J. Freeman and B. Delley, *Phys. Rev. B,***73**,033203 (2006).

[18] D. B. Buchholz, R. P. H. Chang, J.-Y. Song and J. B. Ketterson, *Appl. Phys. Lett.* **87**, 082504 (2005).

[19] Jong-Han Lee, In-Hoon Choi, Sangwon Shin, Sunggoo Lee, J. Lee, Chungnam Whang, Jong-Hyeob Baek, Keun Hwa Chae and Jonghan Songa, *Appl. Phys. Lett,* **90**, 032504 (2007).

[20] C.-F. Yu, T.-J. Lin, S.-J. Sun, and H. Chou, *J. Phys. D* **40**, 6497 (2007).

[21] H. Pan, J. B. Yi, L. Shen, R. Q. Wu, J. H. Yang, J. Y. Lin, Y. P. Feng, J. Ding, L. H. Van, and J. H. Yin, *Phys. Rev. Lett.* **99**, 127201 (2007).

[22] S. Zhou, Q. Xu, K. Potzger, G. Talut, R. Groetzschel, J. Fassbender, M.

Vinnichenko, J. Grenzer, M. Helm, H. Hochmuth, M. Lorenz, M. Grundmann, and H. Schmidt, *Appl. Phys. Lett.* **93**, 232507 (2008).

[23] J. J. Attema, G. A. de Wijs, G. R. Blake, and R. A. de Groot, *J. Am. Chem. Soc.* **127**, 16325 (2005).

[24] Y. Matsumoto, M. Murakami, T. Shono, T. Hasegawa, T. Fukumura, M. Kawasaki, P. Ahmet, T. Chikyow, S.-Y. Koshihara, H. Koinuma, *Science* **291** 854 (2001).

[25] Y. Matsumoto, M. Murakami, K. Hasegawa, T. Fukumura, M. Kawasaki, P. Ahmet, K. Nakajima, T. Chikyow, H. Koinuma, *Appl. Surf. Sci.* **189** 344 (2002).

[26] S.A. Chambers, S. Thevuthasan, R.F.C. Farrow, R.F. Marks, J.U. Thiele, L. Folks, M.G. Samant, A.J. Kellock, N. Ruzycki, D.L. Ederer, U. Diebold, *Appl. Phys. Lett.* **79** 3467 (2001).

[27] S.A. Chambers, C.M. Wang, S. Thevuthasan, T. Droubay, D.E. McCready, A.S. Lea, V. Shutthanandan, C.F. Windisch Jr., *Thin Solid Films* **418** 197 (2002).

[28] S.A. Chambers, T. Droubay, C.M. Wang, A.S. Lea, R.F.C. Farrow, L. Folks, V. Deline, S. Anders, *Appl. Phys. Lett.* **82** 1257 (2003).

[29] S.A. Chambers, R.F.C. Farrow, *MRS Bull.* **28** 729 (2003).

[30] S.A. Chambers, T. Droubay, S.M. Heald, *Phys. Rev. B* **67** 100401(R) (2003).

[31] B.-S. Jeong, Y.W. Heo, D.P. Norton, J.G. Kelly, R. Rairigh, A.F. Hebard, J.D. Bidai, Y.D. Park, *Appl. Phys. Lett.* **84** 2608 (2004).

[32] K.A. Griffin, A.B. Pakhamov, C.M. Wang, S.M. Heald, K.M. Krishnan, *Phys. Rev. Lett.* **94** 157204 (2005).

[33] J.D. Bryan, S.M. Heald, S.A. Chambers, D.R. Gamelin, *J. Am. Chem. Soc.* **126** 11640 (2004)

[34] J.D. Bryan, S.A. Santangelo, S.C. Keveren, D.R. Gamelin, *J. Am. Chem. Soc.* **127** 15568 (2005).

[35] D. H. Kim et al., *Appl. Phys. Lett.* **81**, 13 (2002)

[36] S. R. Shinde, S. B. Ogale, J. S. Higgins, H. Zheng, A. J. Millis, V. N. Kulkarni, R. Ramesh, R. L. Greene, and T. Venkatesan, *Phys. Rev. Lett.* **92** 166601 (2004)

[37] J. M. D. Coey, M. Venkatesan, P. Stamenov, C. B. Fitzgerald, and L. S. Dorneles, *Phys. Rev. B* **72**, 024450 (2005).

[38] N. H. Hong, J. Sakai, N. Poirot, and V. Brizé, *Phys. Rev. B* **73**, 132404 (2006).

[39] N. H. Hong, J. Sakai, and F. Gervais, *J. Magn. Magn. Mater.* **316**, 214 (2007).

[40] N. H. Hong, J. Sakai, and V. Brizé, *J. Phys.: Condens. Matter* **19**, 036219 (2007).

[41] S. D. Yoon, Y. Chen, A. Yang, T. L. Goodrich, X. Zuo, D. A. Arena, K. Ziemer, C. Vittoria, and V. G. Harris, *J. Phys.: Condens. Matter* **18**, L355 (2006).

[42] S. D. Yoon, Y. Chen, A. Yang, T. L. Goodrich, X. Zuo, K. Ziemer, C. Vittoria,

and V. G. Harris, *J. Magn. Magn. Mater.* **309**, 171 (2007).

[43] S. D. Yoon, Y. Chen, A. Yang, T. L. Goodrich, X. Zuo, K. Ziemer, C. Vittoria, and V. G. Harris, *J. Magn. Magn. Mater.* **320**, 597 (2008).

[44] A. K. Rumaiz, B. Ali, A. Ceylan, M. Boggs, T. Beebe, and S. I. Shah, *Solid State Commun.* **144**, 334 (2007).

[45] C. Sudakar, P. Kharel, and R. Suryanarayanan, *J. Magn. Magn. Mater.* **320**, L31 (2008).

[46] Q. Y. Xu, H. Schmidt, S. Q. Zhou, K. Potzger, M. Helm, H. Hochmuth, M. Lorenz, A. Setzer, P. Esquinazi, C. Meinecke, and M. Grundmann, *Appl. Phys. Lett.* **92**, 082508 (2008).

[47] N. H. Hong, N. Poirot, and J. Sakai, *Phys. Rev. B* **77**, 033205 (2008).

[48] A. Sundaresan, R. Bhargavi, N. Rangarajan, U. Siddesh, and C. N. R. Rao, *Phys. Rev. B* **74**, 161306(R) (2006).

[49] C.-F. Yu, T.-J. Lin, S.-J. Sun, and H. Chou, *J. Phys. D* **40**, 6497 (2007).

[50] H. Pan, J. B. Yi, L. Shen, R. Q. Wu, J. H. Yang, J. Y. Lin, Y. P. Feng, J. Ding, L. H. Van, and J. H. Yin, *Phys. Rev. Lett.* **99**, 127201 (2007).

[51] S. Zhou, Q. Xu, K. Potzger, G. Talut, R. Groetzschel, J. Fassbender, M. Vinnichenko, J. Grenzer, M. Helm, H. Hochmuth, M. Lorenz, M. Grundmann, and H. Schmidt, *Appl. Phys. Lett.* **93**. 232507 (2008).

[52] J. J. Attema, G. A. de Wijs, G. R. Blake, and R. A. de Groot, *J. Am. Chem. Soc.* **127**, 16325 (2005).

[53] L. Shen, R. Q. Wu, H. Pan, G. W. Peng, M. Yang, Z. D. Sha, and Y. P. Feng, *Phys. Rev. B* **78**, 073306 (2008).

[54] Kesong Yang, Ying Dai, Baibiao Huang, and M. H. Whangbo, *Appl. Phys. Lett.* **93**, 132507 (2008).

[55] Abdul K. Rumaiz, J. C. Woicik, E. Cockayne, H. Y. Lin, G. Hassnain Jaffari, and S. I. Shah, *Appl. Phys. Lett.* **93**, 262111 (2009).

[56] J. M. D. Coey, Kwanruthai Wongsaprom, J. Alaria, and M. Venkatesan, *J. Phys. D: Appl. Phys*. **41**, 134012 (2008).

[57] Stephen Blundell, Magnetism in Condensed Matter, *Oxford* (2001).

[58] Z. Wilamowski, *Acta Phys. Polon*. A. **77,** 133 (1990).

[59] A. Twardowski, *Mater., Sci. Eng. B* **63,** 96 (1999).

[60] V. F. Sapega, T. Ruf, and M. Cardona, *Solid State Commun.* **114,** 573 (2000).

[61] K. Sato and H. Katayama-Yoshida, *J. J. Appl. Phys.* **39,** L555 (2000).

[62] A. Durst, R. Bhatt, and P. Wolf, *Phys. Rev. B* **65,** 235205 (2002).

[63] D. Angelescu and R. Bhatt, *Phys. Rev. B* **65,** 075221 (2002).

[64] J. Kübler and D. Vigren, *Phys. Rev. B* **11,** 4440 (1975).

[65] J. M. D. Coey, M. Venkatesan, and C. B. Fitzgerald, *Nature Materials* **4**, 173

(2005).

[66] Stefan Hüfner, *Photoelectron Spectroscopy: Principles and Applications,* (Springer-Verlag, Berlin Heidelberg, 1995)

[67] Buddy D. Ratner and David G. Castner, *Surface Analysis-The Principal Techniques*, edited by John C. Vickerman (Wiley, New York, 1997), Ch. 3., pp. 43-98.

[68] B. K. Agarwal, *X-Ray Spectroscopy, 2nd edition*, (Springer-Verlag, Berlin Heidelberg, 1991).

[69] W. Hayes, A.M. *Stoneham Defect and Defect Processes in Nonmetallic Solids* Wiley 1985.

[70] J. H. Schulman, W.D. Compton *Color Centers in Solids* Oxford, Pergamon (1962).

[71] J. M. D. Coey, M. Venkatesan, P. Stamenov, C. B. Fitzgerald, and L. S. Dorneles, *Phys. Rev. B* **72**, 024450 (2005).

[72] C. Di Valentin, G. Pacchioni, A. Selloni, S. Livraghi, E. Giamello, *J. Phys. Chem. B* **109**, 11414 (2005).

[73] Tyuliev G and Angelov S, *Appl. Surf. Sci.* **32,** 381–91 (1988)

[74] M. Naeem, S.K. Hasanain, M. Kobayashi, Y. Ishida, A. Fujimori, S. Buzby, S.I. Shah, *Nanotechnol.* **17**, 2675 (2006).

[75] K.E. Smith, J.L. Mackay, V.E. Henrich, *Phys. Rev. B* **35**, 5822 (1987).

[76] V.E. Henrich, P.A. Cox, *The Surface Science of Metal Oxides*, 1st ed., Cambridge University Press, Cambridge, (1994).

[77] H. Toyosaki, T. Fukumura, Y. Yamada, K. Nakajima, T. Chikyow, T. Hasegawa, H. Koinuma, M. Kawasaki, *Nat. Mater.* 3, 221 (2004).

[78] C. Di Valentin, E. Finazzi, G. Pacchioni, A Selloni, S Livraghi, M C Paganini, E Giamello, *Chemical Physics* **339**, 44–56 (2007).

[79] J. M. Cho, W. J. Yun, J.-K. Lee, H. S. Lee, W. W. So, S. J. Moon, Y. Jia, H. Kulkarni, and Y. Wu, *Appl. Phys. A: Mater. Sci. Process.* **88**, 751 (2007).

[80] Y. Nakaoka and Y. Nosaka, *J. Photochem. Photobiol. A* **110**, 299 (1997).

[81] J. F. Moulder, W.F. Stickle, P.E. Sobol, K.D. Bomben, in: J. Chastain, R.C. King Jr. (Eds.), *Handbook of X-Ray Photoelectron Spectroscopy, Physical Electronics, Inc.*, Minnesota, (1995).

[82] H. Irie, Y. Watanabe, K. Hashimoto, *Chem. Lett.* **32**, 772–773 (2003).

[83] C. Di Valentin, G. Pacchioni, A. Selloni, *Chem. Mater.* **17**, 6656-6665 (2005).